

Robust Heteroclinic Cycles in the One-Dimensional Complex Ginzburg-Landau Equation [★]

D.J.B. Lloyd ^{a,*} A.R. Champneys ^a R.E. Wilson ^a

^a *Bristol Centre for Applied Nonlinear Mathematics and Bristol Laboratory for Advanced Dynamics Engineering, Department of Engineering Mathematics, University of Bristol, Queen's Building, University Walk, Bristol BS8 1TR, UK*

Abstract

Numerical evidence is presented for the existence of stable heteroclinic cycles in large parameter regions of the one-dimensional complex Ginzburg-Landau equation (CGL) on the unit, spatially periodic domain. These cycles connect different spatially and temporally inhomogeneous time-periodic solutions as $t \rightarrow \pm\infty$. A careful analysis of the connections is made using a projection onto 5 complex Fourier modes. It is shown first that the time-periodic solutions can be treated as (relative) equilibria after consideration of the symmetries of the CGL. Second, the cycles are shown to be robust since the individual heteroclinic connections exist in invariant subspaces. Thirdly, after constructing appropriate Poincaré maps around the cycle, a criteria for temporal stability is established, which is shown numerically to hold in specific parameter regions where the cycles are found to be of Shil'nikov type. This criterion is also applied to a much higher-mode Fourier truncation where similar results are found. In regions where instability of the cycles occurs, either Shil'nikov-Hopf or blow-out bifurcations are observed, with numerical evidence of competing attractors. Implications for observed spatio-temporal intermittency in situations modelled by the CGL are discussed.

Key words: Complex Ginzburg-Landau equation, Intermittency, Heteroclinic cycles

PACS:

[★] This work was supported by an EPSRC Research Studentship.

* Corresponding author

Email addresses: david.lloyd@bris.ac.uk (D.J.B. Lloyd),
a.r.champneys@bris.ac.uk (A.R. Champneys), re.wilson@bris.ac.uk (R.E. Wilson).

1 Introduction

Heteroclinic cycles have been observed and analysed in variety of PDEs including the Kuramoto-Sivashinsky equation and Navier-Stokes equations, see [18]. Such cycles are characterised by metastable, recurrent behaviour, made up of long periods of quasi-static regimes with sudden bursts of aperiodic, spatio-temporal evolution, ‘relaxing’ after a while to new quasi-static states. Systems possessing symmetries are often found to admit *robust* heteroclinic cycles that persist under perturbations that respect the symmetry of the system. For example, codimension-two mode interactions in systems with $O(2)$ symmetry, are known to provide a rich variety of robust heteroclinic cycles between equilibria and/or periodic solutions, see [2,29,8,24].

The one-dimensional complex Ginzburg-Landau (CGL) equation on a periodic domain is given by

$$u_t = (1 + i\nu)u_{xx} + Ru - (1 + i\mu)|u|^2u \quad (1)$$

where $u \in \mathbb{C}$, $\nu, \mu, R \in \mathbb{R}$, $x \in [0, 1]$ periodic. It can be shown to be the generic amplitude equation on long space and time scales close to the critical Reynolds number for spatio-temporal pattern formation in fluid dynamics, see Newell *et al.* [32]. More generally, the CGL can be thought of as a normal form for a Hopf bifurcation in a variety of spatially extended systems. The CGL has been used to study many practical problems such as chemical turbulence, Poiseuille flow, Taylor-Couette flow, and Rayleigh-Bénard convection; see Mielke [26] for a review.

Numerous analytical and numerical investigations of the CGL with periodic boundary conditions have been carried out. Analytical results have concentrated on bifurcations from the trivial solution where new solutions can be found from reductions of the CGL to an ODE, see [13]. A closed form solution to the CGL for arbitrary initial data is not known and so numerical investigations provide the only way to fully explore its dynamics away from analytically known special solutions. There have been a few bifurcation sequences mapped out for $\nu = -\mu, R = 0 \dots 100$ ([12,17,27,22]). However, this paper is concerned with exploration away from the line $\nu = -\mu$, where we shall find wide parameter regions where robust heteroclinic cycles occur.

Rodriguez and Schell [35], analysed a two-mode Fourier truncation in an invariant subspace of the CGL but only found structurally unstable heteroclinic cycles. The heteroclinic cycles that we observe in the full PDE are structurally stable (i.e. they persist under perturbations that respect the symmetry of the CGL) and are not described by the truncation of [35]. We find that the minimal truncation necessary to observe these cycles is 5 complex Fourier modes, in which setting we carry out a Shil’nikov-type analysis which shows why the

cycles should be robust.

Our approach to the problem is similar to that of Rucklidge and Matthews [36] who analysed two-dimensional PDEs governing magnetoconvection. We start with a minimal Fourier truncation which possesses the same symmetries as the heteroclinic cycles. We use both numerical continuation and analytical techniques to explore the heteroclinic cycles observed in the truncation. Using the results developed for the low-dimensional truncation we shall attempt to understand the heteroclinic cycles in the full CGL using a high-dimensional truncation. Indeed, we shall find that the 5-mode truncation is qualitatively correct for low R , while additional features occur for larger R . This fact is of no surprise since the length scales in the CGL scale like $R^{1/2}$; see Wilson [34] and Mielke [1].

The paper is outlined as follows. In Section 2 we set out the problem and discuss some of the properties of the observed heteroclinic cycles. This leads us to a minimum Fourier truncation of the CGL that still possesses heteroclinic cycles. A discussion of the numerical techniques is given in Section 2.3. In Section 3 we explore the heteroclinic cycles in the minimal truncation and analyse their persistence and stability using Poincaré-maps constructed around an assumed cycle. In Section 4 we discuss how these results extend to the full PDE and finally, in Section 5, we draw conclusions and suggest avenues for further work.

2 Problem statement

2.1 Relative equilibria

The CGL equation (1) is invariant under the action of two symmetries that are of interest to us:

- \mathbb{S}^1 phase symmetry - $(\alpha \cdot u)(x, t) = e^{i\alpha} u(x, t)$ and,
- $O(2)$ symmetry generated by,
 - translation - $(T_d \cdot u)(x, t) = u(x - d, t)$,
 - reflection - $(R_f \cdot u)(x, t) = u(-x, t)$.

These symmetries mean that non-trivial solutions of the CGL exist on a 2-torus with $\mathbb{S}^1 \times O(2)$ symmetry. In addition, due to the odd power nonlinearity in the CGL, an even (or odd) initial condition yields a solution that remains even (or odd). For example the sub-space of even functions,

$$\mathcal{E} = \{u | R_f \cdot u = u\},$$

remains invariant under the flow of the CGL. By imposing Neumann boundary conditions on $(0, 1/2)$, we can restrict the $\mathbb{S}^1 \times O(2)$ symmetry of the full dynamics to $\mathbb{S}^1 \times \mathbb{Z}_2$ symmetry in an even subspace (see Luce [22] and Doelman [12]).

Let us first describe some known solutions of the CGL. The trivial solution ($u = 0$) is stable for $R < 0$. At $R = 0$ there is a Hopf bifurcation and the trivial solution loses stability to rotating wave solutions of the form

$$u_n(x, t) = r_n e^{i(k_n x - \omega_n t)}, \quad (2)$$

where

$$\begin{aligned} r_n^2 &= R - k_n^2, \\ \omega_n &= k_n^2(\nu - \mu) + \mu R, \end{aligned}$$

and $k_n = 2\pi n$, $n = 0, 1, 2, \dots$. These solutions exist for $R > k_n^2$ and it can be shown that the spatially homogeneous rotating wave (k_0) is the last wave to become unstable as R is increased in the modulationally unstable region $1 + \mu\nu < 0$. This wave becomes unstable to side-band perturbations of spatial frequency $k_m = 2\pi m$, where $m = 1, 2, \dots$, at

$$R_{crit}^{2\pi m} = -(k_m)^2 \frac{(1 + \nu^2)}{2(1 + \mu\nu)}, \quad (3)$$

(see Stuart *et al.* [37]).

Throughout this paper, and without loss of generality, we will take $\mu < 0$ and $\nu > 0$ since (1) is invariant under the transformation $\mu \mapsto -\mu, \nu \mapsto -\nu$, and $u \mapsto \bar{u}$, where an overbar denotes complex conjugation.

Next note that new stable time-periodic solutions of the form,

$$u(x, t) = U(x) e^{i\omega t}, \quad (4)$$

bifurcate off the spatially homogeneous rotating wave at $R_{crit}^{2\pi m}$. Several authors have studied these time-periodic solutions, see [38,33], although the function $U(x)$ is not known in closed form. These solutions have an amplitude, $|U|$, which is spatially dependent, but temporally independent. The function $U(x)$ solves the complex ODE

$$(1 + i\nu)U_{xx} + (R - i\omega)U - (1 + i\mu)|U|^2U = 0. \quad (5)$$

For some parameter regions, as R is increased, time-periodic solutions (4) become unstable and bifurcate to modulated time-periodic solutions where we

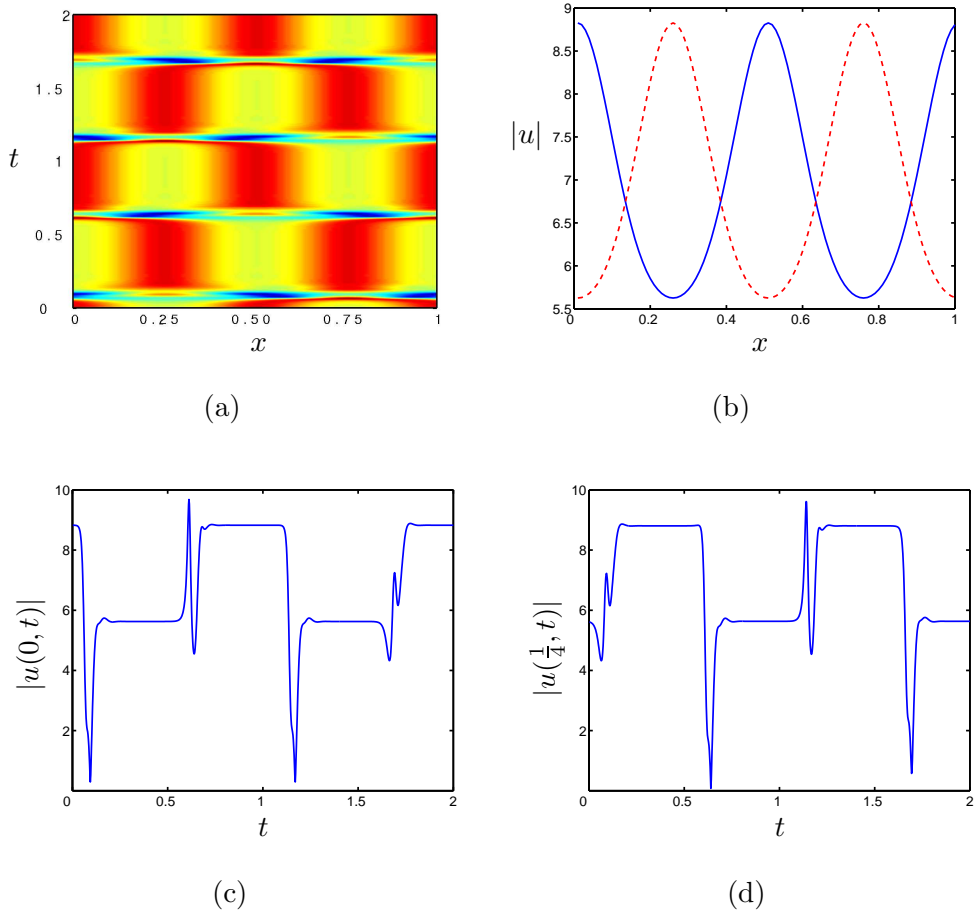


Fig. 1. A typical heteroclinic cycle for $R = 70, \nu = 1, \mu = -4$. (a) Shows a ‘bird’s eye’ view of the amplitude of the CGL solution. Panel (b) shows the amplitude at $t = 1.5$ (dashed line) and at $t = 2$ (solid line). Panels (c) and (d) show time traces at $x = 0$ and $x = 1/4$, respectively

observe temporal oscillations in the amplitude. These new modulated time-periodic solutions break the \mathbb{Z}_2 symmetry and so occur in pairs within the subspace \mathcal{E} . They correspond to two-frequency, quasi-periodic motions on an invariant 2-torus. Eventually, upon increasing R further, the pair of solutions join up by colliding with the spatially homogeneous rotating wave via a homoclinic ‘gluing’ bifurcation [22].

2.2 Preliminary observation of Heteroclinic Cycles

In this section we shall describe a ‘typical’ heteroclinic cycle that we observe in the CGL; see Fig. 1 We solve the CGL by the Crank-Nicolson method with a three-point approximation for second spatial derivatives, see [28]. For Fig. 1, $\Delta x = 5 \times 10^{-3}$ and $\Delta t = 10^{-4}$. Such a scheme is stable and second-order

accurate in both space and time. We observe quasi-static behaviour followed by bursts of aperiodic, spatio-temporal evolution, relaxing to a new quasi-static state. This behaviour is characteristic of heteroclinic dynamics. The quasi-static states are characterised by spatially dependent solutions of time-periodic form (4), possessing \mathbb{Z}_2 symmetry (i.e., they possess spatial reflection about $x = 1/2$, and have spatial frequency $k = 4\pi$). The aperiodic bursts are characterised by initial symmetry breaking (with spatial frequency $k = 2\pi$) of the quasi-static states (4). The ‘equilibria’ forming the heteroclinic points, seen in the amplitude of the solution, are related by a $1/4$ -spatial translation and are in fact fully periodic with \mathbb{S}^1 symmetry. Hence, we should consider them to be relative equilibria. This allows us to consider this heteroclinic cycle as a standard point-to-point cycle within the fixed point subspace of the \mathbb{S}^1 symmetry (see Melbourne *et al.* [24]). The overall solution is not periodic since the solution shifts $\pm 1/4$ in space are seemingly random.

We believe that the chaotic shifting $\pm 1/4$ is due to numerical perturbations around the equilibria of a robust heteroclinic cycle. In Fig 2(a) we see a zoom-in of the L_2 norm as it approaches equilibrium to within numerical error. In Mercader *et al.* [25], they observe *nearly* heteroclinic cycles close to the $1 : 2$ spatial resonance in two-dimensional Rayleigh-Bénard convection without Boussinesq symmetry. They find that these nearly heteroclinic cycles saturate with a finitely long period showing similar behaviour to that in the CGL. A further discussion of the effect numerical error has of the period between burstings is given in Section 3.3.

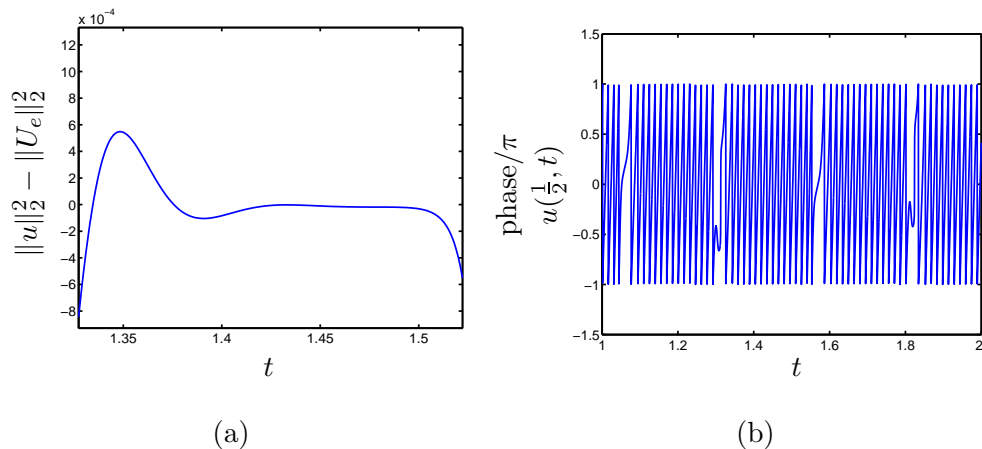


Fig. 2. Panel (a) shows a ‘zoom-in’ of the L_2 norm of the solution as it approaches the time-periodic equilibria $U_e(x)e^{-\omega t}$ to within 10^{-4} . (b) shows the phase/ π of the solution at $x = 1/2$.

Since the invariant sets to which heteroclinic connections occur are time-periodic solutions and so are not known in closed form, we shall take two approaches to gain insight into their existence and stability. The first approach, in Section 3, is based on looking at the minimal ODE projection of

the CGL that still possesses these heteroclinic cycles. The second approach will be to look at a high-dimensional ODE projection of the CGL, using some of the techniques developed for the minimal projection, which we shall discuss Section 4. First let us consider the Fourier projection of the CGL which will be used in both approaches.

2.3 Fourier Projection and Numerical methods

Since we have periodic boundary conditions, it is natural to project the CGL into an infinite-dimensional ODE system using Fourier modes. To do this we write

$$u(x, t) = \sum_{n=-\infty}^{n=+\infty} W_n(t) e^{i2\pi n x}, \quad (6)$$

where the $W_n(t)$ are complex. The Fourier projection (6) applied to (1) yields the infinite-dimensional system of ODEs,

$$\dot{W}_n = (R - (2\pi n)^2(1 + i\nu))W_n - (1 + i\mu) \sum_{k-l+m=n} W_k \bar{W}_l W_m, \quad (7)$$

where $(\cdot) = \frac{d}{dt}$ and an overbar denotes complex conjugation. In order to solve the infinite-dimensional system we shall truncate the Fourier projection to $n = -N, \dots, N$.

The symmetries of the CGL have simple representations in Fourier space with spatial translation and reflection being defined, respectively, as:

$$T_d: W_n \mapsto \exp(i2\pi n d) W_n, \quad (8)$$

$$R_f: W_n \mapsto W_{-n}, \quad (9)$$

with the complex phase \mathbb{S}^1 -symmetry remaining unchanged.

We have chosen to use Matlab's internal 4th-order Runge-Kutta solver to solve the ODE system (7), since it allows for event detection and adaptive time-stepping (useful for heteroclinic cycles since a large amount of the time is spent near the relative equilibria). All computations are made with an relative and absolute error of 10^{-8} .

A standard approach to solving the initial value problem is to look only at solutions in a symmetric (invariant) subspace; see Doelman [12] and Luce [22] (i.e., restrict the flow of the system to one with $\mathbb{S}^1 \times \mathbb{Z}_2$ symmetry). Using a Fourier spectral representation this effectively means the solutions can always be represented as a series of Fourier cosines. We can explicitly decouple the phase symmetry (regardless of the spatial symmetry of the problem) by writing

a solution of (1) as

$$u(x, t) = e^{i\phi(t)} \sum_{n=-\infty}^{n=+\infty} W_n(t) e^{i2\pi n x}, \quad (10)$$

where $W_0 = a_0$ and $W_{|n|} = b_{|n|} + ic_{|n|}$ for $n \neq 0$ and $a_0, b_n, c_n \in \mathbb{R}$. Restricting the solutions of the CGL to a \mathbb{Z}_2 -symmetric subspace implies that $W_{-n} = W_n$.

Projecting (1) onto each mode separately, we obtain the infinite-dimensional system of ODEs

$$i\dot{\phi}(t)W_n + \dot{W}_n = (R - (2\pi n)^2(1 + i\nu))W_n - (1 + i\mu) \sum_{k-l+m=n} W_k \bar{W}_l W_m, \quad (11)$$

governing the W_n 's for $n = 0, 1, 2, \dots, N$. The phase velocity $\dot{\phi}$ is then expressed explicitly by

$$\dot{\phi} = \text{Im} \left(-\frac{(1 + i\mu)}{W_0} \sum_{k-l+m=0} W_k \bar{W}_l W_m \right), \quad (12)$$

which is obtained by taking the imaginary part of the equation for \dot{W}_0 and using the fact that $W_0 = a_0$ is real. Since W_0 appears in the denominator of (12), this method is only valid for dynamics for which W_0 never vanishes.

On making the symmetry assumption $W_{-n} = W_n$, along with the decoupling of the phase, the $(\mathbb{S}^1 \times O(2))$ torus of solutions has been reduced to a locally unique solution, which allows us to use numerical continuation techniques (e.g., AUTO [11]) to look at bifurcation sequences of solutions from the spatially homogeneous rotating wave. Specifically, in this representation the rotating wave is described by an equilibrium point in Fourier space where $W_0 = R^{1/2}$ and $W_n = 0$, for $n \neq 0$. The time-periodic solutions (4) that bifurcate off the rotating wave also correspond to equilibria in Fourier space.

One could carry out a centre-unstable manifold reduction about the bifurcation point where the heteroclinic points come into existence (see Armbruster *et al.* [3]), however even using computer algebra the transformation to eigen-coordinates is highly involved. More crucially, such a reduction would leave a problem in \mathbb{R}^4 , yet (as we shall see) the behaviour observed in a wide region of parameter space requires at least seven phase space dimensions. We still believe though, that close to the bifurcation from the spatially homogeneous state the dynamics are governed by a modified Kuramoto-Sivashinsky equation at $R_{crit}^{2\pi m}$ in which case such a centre-unstable manifold reduction of a resultant Fourier truncation would be possible and beneficial. We shall discuss this further in Section 5.

3 Analysis of the Fourier 5-mode truncation

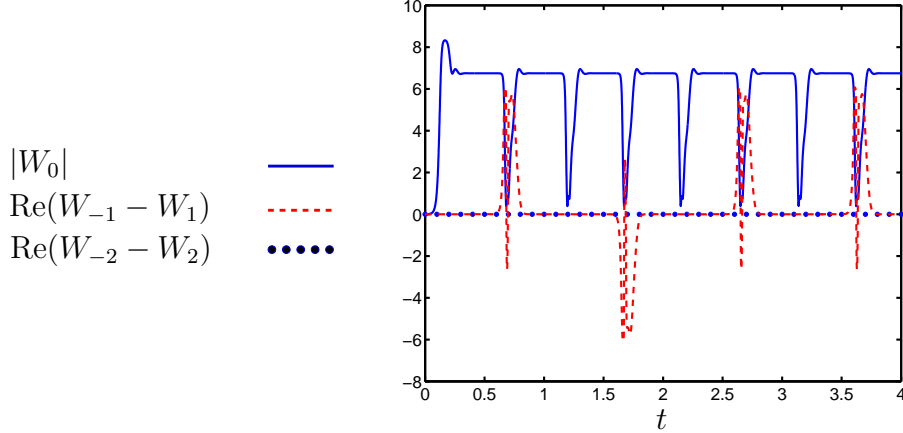


Fig. 3. Heteroclinic cycle in Fourier space, $R = 70$, $\mu = -4$, $\nu = 1$, found by simulation of (11) for $N = 2$, but with phase explicitly decoupled as in (12). The solid line shows evolution of the W_0 mode, the dashed line shows evolution of $\text{Re}(W_{-1} - W_1)$ and the dotted line shows evolution of $\text{Re}(W_{-2} - W_2)$.

In Fig. 3, we show a time evolution of the 5-mode Fourier truncation of the CGL (i.e. $N = 2$), with decoupled phase, starting from a small perturbation of the zero solution. For the same set of parameter values as the simulation of the full PDE, we see qualitatively similar behaviour to the heteroclinic bursting seen in Fig 1. In particular, from Fig. 3 we can see that the spatial average mode (W_0), shown as a solid line, exhibits the standard heteroclinic cycle behaviour. These dynamics are found to be qualitatively similar for $N > 2$ (see Section 4), but we shall concentrate here on the 5-mode truncation.

Our first observation is that the dynamics are strongly attracting. The initial condition used in Fig. 3 was the zero state, and we can see rapid convergence to an attractor. We have observed similarly strong convergence for a variety of other initial conditions including non-symmetric ones and large perturbations from zero.

Our second observation is that the period of bursting is small compared to that of the quiescent phases (time spent at the equilibria). However, the quiescent period is also short (~ 0.5 time units) and one might be fooled into thinking the simulation in Fig. 3 represents periodic motion since most previous numerical observations of heteroclinic cycles have produced large periods between bursting. As we shall see in Section 3.3 though, the bursting occurs in invariant subspaces which the numerical simulations approach to within numerical error ($\sim 10^{-8}$). In these invariant subspaces we have a connection from an unstable equilibrium to a stable one, but the leading destabilising eigenvalue (λ) is large and, as we shall show in Section 3.2, the time spent at

the equilibria is $O(\lambda^{-1})$ before numerical error causes the next burst to occur.

3.1 Existence of Heteroclinic cycles

Some other key observations about the heteroclinic cycles can be made by looking at the two other quantities plotted in Fig. 3, $\text{Re}(W_{-1} - W_1)$ and $\text{Re}(W_{-2} - W_2)$. These quantities correspond to $W_{-1} = W_1$ and $W_{-2} = W_2$ symmetries. It is clear from Fig. 3 that the quantity $\text{Re}(W_{-2} - W_2) = 0$ for all time with $W_{-2} \neq 0$ and $W_2 \neq 0$. This implies, and can be checked numerically, that $W_{-2}(t) = W_2(t)$ is a spatial symmetry of the heteroclinic cycles. (Without explicitly decoupled phase we would find that the quantity $|W_{-2}| - |W_2| = 0$ for all time, instead. Throughout this section though, we shall assume that we are in the fixed point subspace of the complex phase and so assume the complex phase has been decoupled.) The other quantity, $\text{Re}(W_{-1} - W_1)$ is zero at equilibrium and for exactly half the heteroclinic connections. Hence exactly half of the heteroclinic connections lie in the invariant subspace where $W_{-n} = W_n$, $n \neq 0$: this is the (even) \mathbb{Z}_2 restriction discussed in Section 2.2. If we plotted $\text{Re}(W_{-1} + W_1)$ then we would see the same as for $\text{Re}(W_{-1} - W_1)$ but, the quantity would be zero during the other half of heteroclinic connections. This then gives us another ('odd') \mathbb{Z}_2 -invariant subspace where $W_{-2} = W_2, W_{-1} = -W_1$. We shall refer to the even subspace as $Z_2 = \{W_{-1} = W_1, W_{-2} = W_2\}$ and the odd one as $\tilde{Z}_2 = \{W_{-1} = -W_1, W_{-2} = W_2\}$. Both subspaces intersect at the equilibria where $W_{-1} = W_1 = 0$ allowing for structurally stable heteroclinic cycles to exist to such equilibria within either subspace.

In order to understand the heteroclinic cycles better, it is clear that we must look at the \mathbb{Z}_2 -subspace restrictions. We shall just consider Z_2 since the corresponding solutions in \tilde{Z}_2 can be found by a simple spatial translation of $1/2$. Therefore, we reduce the 5 Fourier mode truncation to just looking at 3 Fourier modes (W_0, W_1 and W_2).

We shall first look at the equilibria which are invariant under $T_{1/2}$ (i.e., $T_{1/2}(W_0, W_1, W_2) \mapsto (W_0, -W_1, W_2)$), which implies that $W_{-1} = W_1 = 0$. Hence the equations reduce to (in Fourier space without decoupled phase),

$$\begin{aligned} \dot{W}_0 &= RW_0 - (1 + i\mu) \left\{ W_0 \left(|W_0|^2 + 4|W_2|^2 \right) + 2W_2^2 \overline{W_0} \right\}, \\ \dot{W}_2 &= (R - (4\pi)^2(1 + i\nu))W_2 - (1 + i\mu) \left\{ W_2(3|W_2|^2 + 2|W_0|^2) + W_0^2 \overline{W_2} \right\}, \end{aligned} \tag{13}$$

where bar denotes complex conjugate. The first thing to note here is that the equations are invariant under a spatial shift of a $1/4$ (i.e., $T_{1/4}(W_0, W_2) \mapsto (W_0, -W_2)$). Consequently, any linearisation must also be invariant under such

action and we should expect steady bifurcations to be pitchforks which break this symmetry. The eigenvalues associated with the W_0 and W_2 modes are called radial eigenvalues i.e., the eigenvalues are the same for both solutions related by $T_{1/4}$.

If we explicitly decouple the phase as in (12), we get

$$\begin{aligned}
\dot{a}_0 &= Ra_0 - a_0^3 - 2a_0b_2^2 - 6a_2^2a_0 + 4\mu a_2b_2a_0, \\
\dot{a}_2 &= Ra_2 - (4\pi)^2a_2 + (4\pi)^2\nu b_2 - 3a_2a_0^2 - 7a_2b_2^2 - 3\mu a_2^2b_2 + \mu b_2^3 - 3a_2^3, \\
\dot{b}_2 &= Rb_2 - (4\pi)^2b_2 - (4\pi)^2\nu a_2 + 3\mu a_2^3 - b_2a_0^2 - 2\mu a_2a_0^2 + a_2^2b_2 - 3b_2^3 - \mu a_2b_2^2,
\end{aligned} \tag{14}$$

where $W_0 = a_0$ and $W_2 = a_2 + ib_2$. We can see that the first bifurcation off the spatially homogeneous rotating wave ($W_0 = +\sqrt{R}, W_2 = 0$) occurs at $R_{crit}^{4\pi}$. Specifically, if we linearise about the spatially homogeneous state we get the eigenvalues, $-2R, -(R + (4\pi)^2) \pm \sqrt{R^2 - 2(4\pi)^2\nu\mu R - (4\pi)^4\nu^2}$, and we may observe that the wave loses stability at $R = R_{crit}^{4\pi}$. At this bifurcation point, the spatially homogeneous rotating wave undergoes a supercritical (for the parameters we are interested in) pitchfork bifurcation to two new equilibria, ξ_1 and ξ_2 , which are related by a $1/4$ spatial shift (i.e., $T_{1/4}\xi_1 = \xi_2$). Both equilibria must bifurcate off with the same stability and in this reduction both are asymptotically stable since we have no 2π -periodic destabilising sideband-perturbation associated with the W_1 mode.

As R is increased we eventually find that for some parameter values, the equilibria (ξ_1, ξ_2) undergo supercritical Hopf bifurcations. Again both have the same stability and bifurcate at the same point in parameter space. Since the W_1 mode is zero for the emanating limit cycles, this throws up the possibility of a Shil'nikov-Hopf bifurcation of the heteroclinic cycles; see Section 3.3 below.

We shall now turn to numerical continuation to assess the stability of the relative equilibria with respect to full perturbations in Z_2 . Fig. 4 shows the bifurcation diagram of equilibria in the Z_2 subspace for $\nu = 1, \mu = -4$. Between $R = 0$ and $R = R_{crit}^{2\pi} \approx 13.16$, the spatially homogeneous rotating wave is stable (solid line). At $R = R_{crit}^{2\pi}$ there is a supercritical pitchfork bifurcation to the time-periodic solutions, related by a $1/2$ spatial shift (i.e. $W_0 \neq 0, W_1 \mapsto -W_1, W_2 \mapsto W_2$). These new solutions are also stable in the full truncation and eventually undergo a supercritical Hopf-bifurcation at $R_{Hopf}^{2\pi}$. The limit-cycles eventually connect to the spatially homogeneous rotating wave in a homoclinic gluing bifurcation as described by Luce [22].

At $R = R_{crit}^{4\pi} \approx 52.64$ two new equilibria (ξ_1 and ξ_2) bifurcate off the rotating wave which are, initially, unstable since the rotating wave is unstable

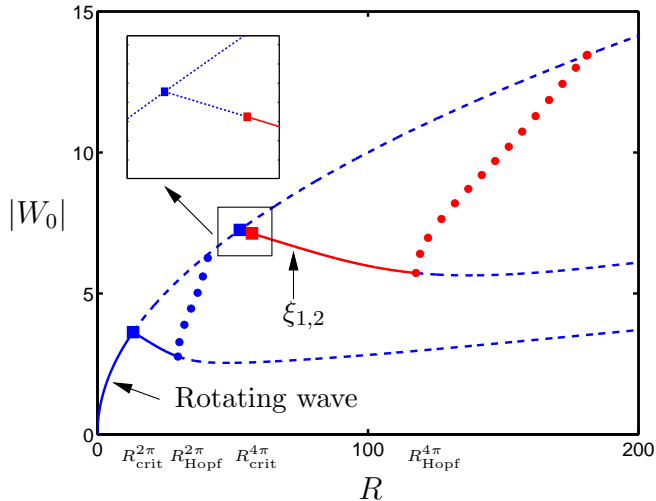


Fig. 4. Bifurcation diagram in the subspace Z_2 for $\nu = 1, \mu = -4$. Solid lines denote stable equilibria and dashed lines unstable ones. Here stability is calculated with respect to full perturbations in Z_2 for which $W_1 \neq 0$ in general. Squares denote pitchfork bifurcations. Circles denote periodic solutions emanating from a Hopf bifurcation. The heteroclinic points correspond to the two equilibria bifurcating off the spatially homogeneous rotating wave at $R_{crit}^{4\pi}$ for the sideband perturbation $k_m = 4\pi$ (both equilibria are initially unstable). At the square on the ξ_1, ξ_2 branch, one equilibrium ξ_2 becomes stable with the other equilibrium ξ_1 remaining unstable (see insert). Other equilibria solutions bifurcate off when the equilibrium ξ_2 becomes stable (not shown).

for $R = R_{crit}^{4\pi}$. This initial instability does not last long for one branch of solutions (corresponding to ξ_2), which becomes stable at $R \approx 57.11$. At this point another unstable branch of solutions bifurcates off (not shown). This situation (ξ_2 stable and ξ_1 unstable) continues until the Hopf-bifurcation at $R = R_{Hopf}^{4\pi} \approx 117.13$. Since the Hopf bifurcation is supercritical the equilibria ‘transfer’ their stability to the resulting limit cycles and so we have one stable and one unstable limit cycle. Clearly, having one stable and one unstable branch of solutions, related by symmetry, is due to the eigenvalues associated with the W_1 mode not being invariant under the spatial shift of a $1/4$ (unlike the W_0 and W_2 modes). Hence, the eigenvectors associated with the W_1 -mode are orthogonal to the eigenvectors associated with the W_0 and W_2 -modes. This fact will be important for us in calculating asymptotic stability of the heteroclinic cycles, see Section 3.2. One would hope that it would be possible to start at the unstable equilibrium, say ξ_1 , and evolve to the stable equilibrium, ξ_2 . Indeed this is the case and we have found that this connection is structurally stable in the Z_2 -subspace.

To show that if there exists a connection taking us from ξ_1 to ξ_2 in the Z_2 -subspace then there is a connection back to ξ_1 we now consider the other Z_2 -invariant subspace \tilde{Z}_2 . It is straightforward to show that equilibria $\xi_1, \xi_2 \in \tilde{Z}_2 \cap Z_2$, moreover, a transformation $T_{1/4}$ maps $\xi_1 \rightarrow \xi_2$ and maps any solution

$u(t) \in \{W_0, W_1, W_2\} \in Z_2$ to a solution $\tilde{u}(t) = T_{1/4}u(t) \in \tilde{Z}_2$. Hence, the bifurcation diagram of equilibria in \tilde{Z}_2 is identical to that in Fig. 4, but along the branch if ξ_1 is stable and ξ_2 is unstable with respect to perturbations in Z_2 , precisely the opposite is true in \tilde{Z}_2 . Most importantly, the existence of a structurally stable heteroclinic orbit within Z_2 , $h : \xi_1 \rightarrow \xi_2$, implies that there exists another structurally stable heteroclinic connection in \tilde{Z}_2 since $\xi_2 = T_{1/4}\xi_1 \rightarrow T_{1/4} \circ (T_{1/4}\xi_1) = \xi_1$. Therefore, the heteroclinic cycle in the full 5 mode truncation is $\xi_1 \rightarrow \xi_2 \rightarrow \xi_1$. Note that $T_{1/4}\xi_1 = T_{3/4}\xi_1$ so in the full system one can shift either to the right or left, to connect back to the other equilibrium (i.e. $\xi_1 \rightarrow T_{3/4}\xi_1 = \xi_2 \rightarrow T_{3/4} \circ (T_{3/4}\xi_1) = \xi_1$).

Pictorially, we can consider the heteroclinic cycle existing in two subspaces (shown as planes in Fig 5) which are orthogonal to one another with the heteroclinic connections existing in either subspace. Of course, in the full PDE these subspaces are infinite-dimensional.

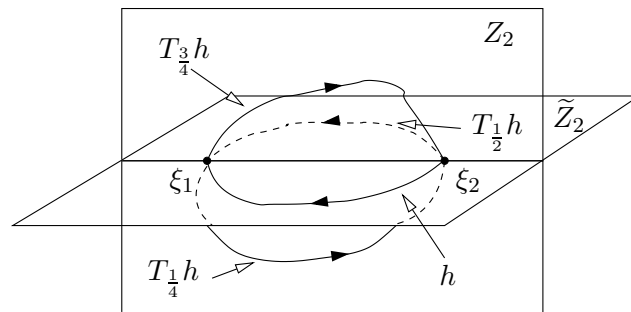


Fig. 5. Pictorial representation of the heteroclinic cycle in both Z_2 and \tilde{Z}_2 -subspaces.

One question that needs to be asked is how large is the parameter space where the situation of Fig. 5 exists in the Z_2 subspace. Using numerical continuation, we can answer this question by continuing in two parameters the locus of the bifurcation point where one branch becomes stable. In Fig. 6, we show a two-parameter plot in the (R, ν) -plane showing the region of existence of structurally stable heteroclinic connections for $\mu = -4$. Other choices of μ produce similar diagrams but to simplify the presentation of the dynamics of the CGL we shall stick to $\mu = -4$. The circles denote the locus of the Hopf bifurcation passing through this region. Somewhere in this region, heteroclinic cycles become asymptotically stable and so we might be able to observe them numerically. Conditions for asymptotic stability of the heteroclinic cycles and what happens when we lose stability are discussed in the following section.

3.2 Stability and other dynamics near the Heteroclinic cycles

An important feature of robust heteroclinic cycles is that they attract nearby dynamics, that is they are asymptotically stable. The standard approach to

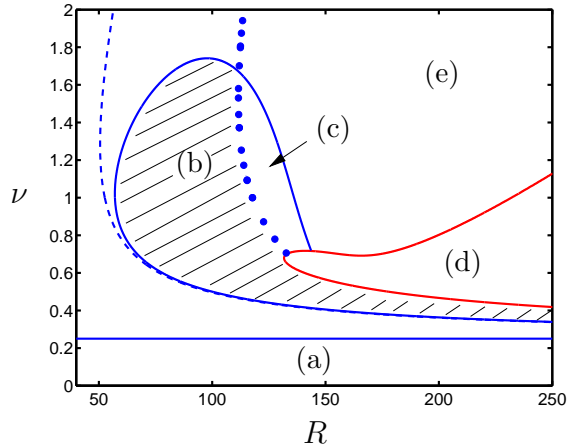


Fig. 6. Existence region of structurally stable heteroclinic connections for $\mu = -4$ in the 5 Fourier mode truncation (shown as the shaded region (b)). (a) Modulational stable region $1 + \mu\nu > 0$, the bifurcation locus for $R_{crit}^{4\pi}$ is the dashed line, the Hopf-bifurcation locus is shown as circles, (c) is the region where we have possible heteroclinic connections between limit-cycles and (d) is where stable 4π -time-periodic solutions can be found. Region (e) is where the limit-cycles are stable. More details inside the shaded region (b) are given in Fig. 11.

analysing stability of heteroclinic cycles is based on the construction of the Poincaré return map for the flow near the cycle. The symmetry of the problem complicates issues somewhat producing an unusual result in that stability is governed by eigenvalues which are not necessarily the closest to the imaginary axis (as for standard homoclinic stability). The general theory of Krupa and Melbourne [19] is applicable here, but in order to find out what happens when we lose asymptotic stability, we shall also construct approximate Poincaré maps from first principles. The analysis will also help us explain the numerical simulations and short period of the heteroclinic cycles. We follow similar Shil'nikov-type constructions in Glendinning and Sparrow [14] and Hirschberg and Knobloch [15]. The approach is to linearise the flow close to ξ_1 and ξ_2 which can be justified by (generalisation of) the Hartman and Grobman theorem provided the equilibria remain hyperbolic. Rigorous justification of this approach for general non-equivariant systems has been proved by Deng [10] and Lin [21].

Close to $R_{crit}^{4\pi}$, we find that all the leading eigenvalues in the Z_2 and \tilde{Z}_2 -subspaces are real and so the results from the $O(2)$ -equivariant normal form apply (Armbruster *et al.* [2] and Campbell and Holmes [8]). Campbell and Holmes find that the stability of the heteroclinic cycle is governed by the ratio $\rho = -\alpha/\lambda$, where α is the maximum eigenvalue at ξ_2 in the Z_2 -subspace and λ is the unstable eigenvalue at ξ_1 in Z_2 . If $\rho > 1$ then the cycle is found to be asymptotically stable. As ρ passes through unity, Armbruster *et al.* [2] find that an unstable, modulated travelling wave bifurcates off the heteroclinic cycle. As R is increased further away from $R_{crit}^{4\pi}$, the leading eigenvalues become

complex conjugate and so the 1:2 mode interaction $O(2)$ -equivariant normal form results of Armbruster *et al.* no longer apply.

Since general parameterised expressions for the eigenvalues at ξ_1 and ξ_2 are cumbersome, we shall start by looking at the stability of our ‘typical’ heteroclinic cycle for $R = 70, \mu = -4, \nu = 1$ where the leading stable eigenvalues are complex conjugate. In the 5-mode truncation the linearisation around either equilibrium yields the following eigenvalues in the fixed point subspace of the complex phase (\mathbb{S}^1) symmetry. The eigenvalues associated with the W_{-1} and W_1 modes are

$$\lambda_1 = +82.3, \lambda_{2,3} = -92.5 \pm 24.8i, \lambda_4 = -175.9,$$

and the ‘radial’ eigenvalues associated with the W_0, W_{-2} and W_2 modes are

$$\lambda_5 = 0, \lambda_{6,7} = -44.8 \pm 74.7i, \lambda_8 = -356.2, \lambda_9 = -367.1.$$

Let the corresponding eigenvectors be $\mathbf{v}_1 \dots \mathbf{v}_9$. The first observation is that we have a Shil’nikov saddle-focus situation with a 1D unstable manifold. The zero eigenvalue is due to the $O(2)$ symmetry and so there is no motion in the direction corresponding to that eigenvector. Hence we can ignore this eigendirection when considering the stability and the dynamics near the heteroclinic cycle. Other eigenvalues that we can ignore (somewhat anticipating the result) are λ_4, λ_8 and λ_9 since they are not the leading stable eigenvalues (i.e., closest to the imaginary axis) in either the Z_2 or \tilde{Z}_2 subspaces.

In order to carry out the Poincaré map analysis, we now consider the eigencoordinates $(a_1, r_1, \theta_1, r_2, \theta_2)$, where a_1 is the coordinate in the direction of \mathbf{v}_1 , $(r_1 \cos \theta_1, r_1 \sin \theta_1)$ is in the direction spanned by \mathbf{v}_2 and \mathbf{v}_3 , and $(r_2 \cos \theta_2, r_2 \sin \theta_2)$ is in the direction spanned by \mathbf{v}_6 and \mathbf{v}_7 . We shall assume that in Z_2 at equilibrium ξ_1 , we have $r_2 = \theta_2 = 0$ and at equilibrium ξ_2 , we have $a_1 = 0$. This is consistent with the heteroclinic cycle problem and can be considered as another representation of the Z_2 -subspace. The representation of \tilde{Z}_2 at ξ_1 is $a_1 = 0$ and at ξ_2 the representation is $r_2 = \theta_2 = 0$. Hence, we assume the linearisation (in polar co-ordinates) of the flow about ξ_1 or ξ_2 , in the form $\dot{a}_1 = \lambda_1 a_1, \dot{r}_1 = \gamma r_1, \dot{\theta}_1 = \Omega, \dot{r}_2 = \alpha r_2, \dot{\theta}_2 = \beta$ where $\lambda_{6,7} = \gamma \pm i\Omega$ and $\lambda_{2,3} = \alpha \pm i\beta$. Here $\lambda_1 > 0 > \text{Re}(\lambda_{6,7}) > \text{Re}(\lambda_{2,3})$.

Take one of the invariant subspaces, say Z_2 . At ξ_1 is unstable with $r_2 = 0$, and ξ_2 is stable with $a_1 = 0$. We let $\eta > 0$ be a small real number and we define the following three Poincaré sections, shown schematically in Fig. 7.

Let $x_0, y_0, z_0 \in \mathbb{R}^5$ define points belonging to the connecting orbits $h : \xi_1 \rightarrow \xi_2$ and $T_{1/4}h : \xi_2 \rightarrow \xi_1$ (or $T_{3/4}h : \xi_2 \rightarrow \xi_1$), with $|x_0 - \xi_1| = |y_0 - \xi_1| = |z_0 - \xi_2| = \eta \ll 1$. We define y_0^\pm and z_0^\pm as regions within the points where

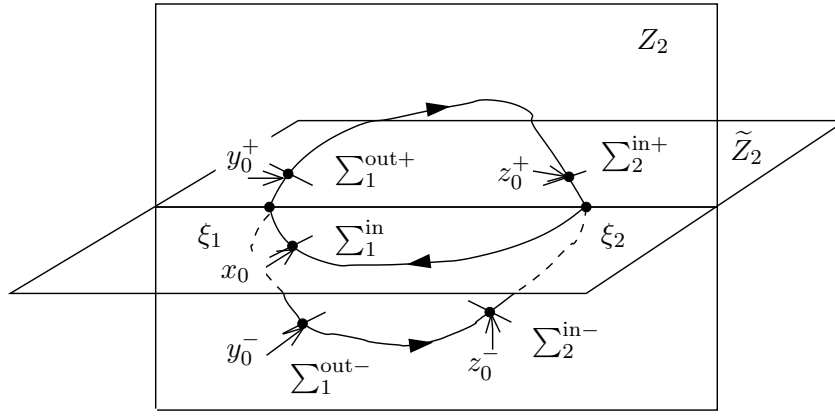


Fig. 7. Pictorial representation of the heteroclinic connections.

y_0^\pm is determined by the sign of a_1 , z_0^+ is determined by $0 < \theta_1 < \pi$ and z_0^- is determined by $\pi < \theta_1 < 2\pi$. This restriction on θ_1 implies that in Cartesian coordinates, z_0^+ has $a_3 = r_1 \sin \theta_1 > 0$ and z_0^- has $a_3 < 0$.

Around ξ_1 we define the Poincaré sections,

$$\begin{aligned} \Sigma_1^{\text{in}} : x_0 + \{(a_1, r_1, \theta_1, r_2, \theta_2) \mid -\delta \leq a_1 \leq \delta, r_1 = \eta, -\delta \leq \theta_1 \leq \delta, \\ 0 \leq r_2 \leq \delta, 0 \leq \theta_2 \leq 2\pi\}, \\ \Sigma_1^{\text{out}\pm} : y_0 + \{(a_1, r_1, \theta_1, r_2, \theta_2) \mid a_1 = \pm\eta, 0 \leq r_1 \leq \delta, 0 \leq \theta_1 \leq 2\pi, 0 \leq r_2 \leq \delta, \\ 0 \leq \theta_2 \leq 2\pi\}, \quad (15) \end{aligned}$$

and around ξ_2 ,

$$\begin{aligned} \Sigma_2^{\text{in}\pm} : z_0 + \{(a_1, r_1, \theta_1, r_2, \theta_2) \mid -\delta \leq a_1 \leq \delta, r_1 = \eta, \theta^* - \delta \leq \theta_1 \pm \pi \leq \theta^* + \delta, \\ 0 \leq r_2 \leq \delta, 0 \leq \theta_2 \leq 2\pi\}, \quad (16) \end{aligned}$$

here $0 < \delta \ll \eta$ is a small real number. We could of course, factor out the symmetry of the heteroclinic cycles by identifying Poincaré sections at the different heteroclinic connections by using the symmetry of $T_{1/4}$. This would result in a system possessing one homoclinic orbit instead of a homoclinic cycle. This method is known as the orbit space reduction. We shall however, stick to this more intuitive choice of Poincaré sections.

Let U be a neighbourhood of the origin (x_0) in Σ_1^{in} . If U is sufficiently small then all trajectories starting in U either converge to ξ_1 (this happens for all points with $a_1 = 0$) or hit one of the other sections, $\Sigma_2^{\text{in}+}$ or $\Sigma_2^{\text{in}-}$. With a slight abuse of notation, we write the map from ξ_1 to ξ_2 as $g(\mathbf{a})$ instead of $g(x_0 + \mathbf{a})$. We shall also use the notation $\text{Fix}(Z_2)$ to define the fixed point subspace of Z_2 i.e at ξ_1 , $r_2 = \theta_2 = 0$ and at ξ_2 , $a_1 = 0$.

For all initial conditions in $U \setminus T_{1/4} \text{Fix}(Z_2)$ the map g^2 is the return map generated by the flow along the heteroclinic cycle the connections $\xi_1 \rightarrow \xi_2 \rightarrow \xi_1$ defined by $T_{1/4}$ (or $T_{3/4}$).

The local map ψ at ξ_1 under the linear flow of initial conditions $(a_1, \eta, \theta_1, r_2, \theta_2)$, is given by

$$\psi^\pm : \Sigma_1^{in} \mapsto \Sigma_1^{out\pm} : (a_1, \eta, \theta_1, r_2, \theta_2) \mapsto (\text{sgn}(a_1)\eta, \eta e^{\gamma T}, \Omega T + \theta_1, r_2 e^{\alpha T}, \beta T + \theta_2) + \text{h.o.t.}, \quad (17)$$

where $T = \lambda_1^{-1} \ln(\eta/|a_1|)$. In Cartesian co-ordinates $(a_1, a_2, a_3, a_4, a_5)$, ψ becomes, to leading order

$$\begin{aligned} \psi : \Sigma_1^{in} \mapsto \Sigma_1^{out\pm} : (a_1, \eta, a_3, a_4, a_5) \mapsto & \left(\text{sgn}(a_1)\eta, \right. \\ & \eta \left(\frac{\eta}{|a_1|} \right)^{\gamma/\lambda_1} \cos \left(\frac{\Omega}{\lambda_1} \ln \left(\frac{\eta}{|a_1|} \right) \right), \eta \left(\frac{\eta}{|a_1|} \right)^{\gamma/\lambda_1} \sin \left(\frac{\Omega}{\lambda_1} \ln \left(\frac{\eta}{|a_1|} \right) \right), \\ & \left. \left(\frac{\eta}{|a_1|} \right)^{\alpha/\lambda_1} \left[a_4 \cos \left(\frac{\beta}{\lambda_1} \ln \left(\frac{\eta}{|a_1|} \right) + \theta_2^* \right) - a_5 \sin \left(\frac{\beta}{\lambda_1} \ln \left(\frac{\eta}{|a_1|} \right) + \theta_2^* \right) \right], \right. \\ & \left. \left(\frac{\eta}{|a_1|} \right)^{\alpha/\lambda_1} \left[a_4 \sin \left(\frac{\beta}{\lambda_1} \ln \left(\frac{\eta}{|a_1|} \right) + \theta_2^* \right) + a_5 \cos \left(\frac{\beta}{\lambda_1} \ln \left(\frac{\eta}{|a_1|} \right) + \theta_2^* \right) \right] \right). \quad (18) \end{aligned}$$

For the global map taking us from ξ_1 to ξ_2 in a neighbourhood of the robust heteroclinic connection h , we assume the connection occurs in the Z_2 -subspace. Moreover, we consider the connection from $\Sigma_1^{out\pm}$ to $\Sigma_2^{in\pm}$, hence our global map ϕ maps $\text{Fix}(Z_2) \cap \Sigma_1^{out\pm} \mapsto \text{Fix}(Z_2) \cap \Sigma_2^{in\pm}$. This map must therefore be a diffeomorphism of the form:

$$\phi : (\pm\eta, \tilde{a}_2, \tilde{a}_3, \tilde{a}_4, \tilde{a}_5) \mapsto (\pm(f_1\tilde{a}_4 + f_2\tilde{a}_5), \eta, \pm f_3, f_4, f_5), \quad (19)$$

where $f_i = f_i(\tilde{a}_2, \tilde{a}_3, \tilde{a}_4, \tilde{a}_5)$, $i = 1 \dots 5$ are smooth functions for which we make the non-degeneracy assumptions that f_1 and f_2 have nonzero constant terms. The condition that $f_i(0, 0, 0, 0) \neq 0$, $i = 3 \dots 5$ can easily be expressed as a condition on the variational equation (Melnikov integral) for the connection $\xi_1 \rightarrow \xi_2$. Although we do not have explicit expressions for the functions f_i in this mapping, their arguments are vanishingly small as $\eta \rightarrow 0$. We therefore expand them in a Taylor series about $(a_2, a_3, a_4, a_5) = (0, 0, 0, 0)$. Note that $f_1(0, 0, 0, 0) = f_2(0, 0, 0, 0) = 0$, $f_3(0, 0, 0, 0) = \pm\hat{a}_3$, $f_i(0, 0, 0, 0) = \hat{a}_i$, $i = 4, 5$, where $(0, \eta, \pm\hat{a}_3, \hat{a}_4, \hat{a}_5)$ are the coordinates of the intersection of the heteroclinics with $\Sigma_2^{in\pm}$ and $|\hat{a}_3|, |\hat{a}_4|, |\hat{a}_5| \sim O(\delta)$.

If we compose the map $g = T_{1/4}\phi \circ \psi$, it takes the form:

$$g(a_1, a_3, a_4, a_5) = (\text{sgn}(a_1)h_1|a_1|^\rho \cos(\Delta_1 \ln|a_1| + \Delta_2), \text{sgn}(a_1)h_2, h_3, h_4).$$

Here Δ_i are $O(1)$ constants, $h_i = h_i(a_1, a_3, a_4, a_5)$, $i = 1 \dots 4$ are smooth functions and $\rho = -\alpha/\lambda_1$. For asymptotic stability we need to bound $|h_i(a_1, a_3, a_4, a_5)| \leq K|a_1|^\rho$, $i = 2, 4$ and $|h_1(a_1, a_3, a_4, a_5)| \leq K$ where $(a_1, a_3, a_4, a_5) \in U$. Hence, for a general choice of (a_1, a_3, a_4, a_5) there exists

a constant $L > 0$ such that $L \leq h_1(a_1, a_3, a_4, a_5)$. We can now see that if $\rho > 1$ then the heteroclinic cycle should be asymptotically stable. Note that is this criteria is a necessary and sufficient condition for asymptotic stability. For our typical heteroclinic cycle ($R = 70, \nu = 1, \mu = -4$) the quantity $\rho = \alpha/\lambda_1 \approx 1.12$, which implies stability. But what if $\alpha/\lambda_1 < 1$?

If we assume that the heteroclinic connection pierces Σ_1^{in} at $(0, \eta, \hat{a}_3, \hat{a}_4, \hat{a}_5)$, after some linearisation, the return map g to lowest order is given by,

$$\begin{aligned}
g : (a_1, a_3, a_4, a_5) &\mapsto (\text{sgn}(a_1) \times \\
&\left\{ \Delta_1 \left(\frac{\eta}{|a_1|} \right)^{\alpha/\lambda_1} \left[a_4 \cos \left(\frac{\beta}{\lambda_1} \ln \left(\frac{\eta}{|a_1|} \right) + \theta_2^* \right) - a_5 \sin \left(\frac{\beta}{\lambda_1} \ln \left(\frac{\eta}{|a_1|} \right) + \theta_2^* \right) \right] \right. \\
&+ \Delta_2 \left(\frac{\eta}{|a_1|} \right)^{\alpha/\lambda_1} \left[a_4 \sin \left(\frac{\beta}{\lambda_1} \ln \left(\frac{\eta}{|a_1|} \right) + \theta_2^* \right) + a_5 \cos \left(\frac{\beta}{\lambda_1} \ln \left(\frac{\eta}{|a_1|} \right) + \theta_2^* \right) \right] \left. \right\}, \\
&\text{sgn}(a_1)(\hat{a}_3 + \Delta_3 \Pi_1 + \Delta_4 \Pi_2 + \Delta_5 \Pi_3 + \Delta_6 \Pi_4), \\
&\hat{a}_4 + \Delta_7 \Pi_1 + \Delta_8 \Pi_2 + \Delta_9 \Pi_3 + \Delta_{10} \Pi_4, \\
&\hat{a}_5 + \Delta_{11} \Pi_1 + \Delta_{12} \Pi_2 + \Delta_{13} \Pi_3 + \Delta_{14} \Pi_4), \quad (20)
\end{aligned}$$

where,

$$\begin{aligned}
\Pi_1 &= \eta \left(\frac{\eta}{|a_1|} \right)^{\gamma/\lambda_1} \cos \left(\frac{\Omega}{\lambda_1} \ln \left(\frac{\eta}{|a_1|} \right) \right), \\
\Pi_2 &= \eta \left(\frac{\eta}{|a_1|} \right)^{\gamma/\lambda_1} \sin \left(\frac{\Omega}{\lambda_1} \ln \left(\frac{\eta}{|a_1|} \right) \right), \\
\Pi_3 &= \left(\frac{\eta}{|a_1|} \right)^{\alpha/\lambda_1} \left[a_4 \cos \left(\frac{\beta}{\lambda_1} \ln \left(\frac{\eta}{|a_1|} \right) + \theta_2^* \right) - a_5 \sin \left(\frac{\beta}{\lambda_1} \ln \left(\frac{\eta}{|a_1|} \right) + \theta_2^* \right) \right], \\
\Pi_4 &= \left(\frac{\eta}{|a_1|} \right)^{\alpha/\lambda_1} \left[a_4 \sin \left(\frac{\beta}{\lambda_1} \ln \left(\frac{\eta}{|a_1|} \right) + \theta_2^* \right) + a_5 \cos \left(\frac{\beta}{\lambda_1} \ln \left(\frac{\eta}{|a_1|} \right) + \theta_2^* \right) \right], \quad (21)
\end{aligned}$$

and $\Delta_1 = f_1(0)$ and $\Delta_2 = f_2(0)$.

If we assume that for small a_1 , $a_3 \approx \pm \hat{a}_3$, $a_4 \approx \hat{a}_4$ and $a_5 \approx \hat{a}_5$, then the essential dynamics of (20) is given by the map

$$a_1 \mapsto \text{sgn}(a_1) \times \left(|a_1|^\rho \Lambda \cos \left(\frac{\beta}{\lambda_1} \ln(|a_1|) + \Phi \right) \right), \quad (22)$$

where Λ and Φ are arbitrary constants. This map is similar to the standard Shil'nikov map at homoclinicity and so for $\rho < 1$ we have an infinite number of (saddle) periodic orbits. In the usual 3D case (e.g Glendinning and Sparrow [14]) the homoclinic orbit (here a heteroclinic cycle) would be destroyed

as a parameter is varied (an additive parameter on the r.h.s of (20)). Here however, owing to the symmetry properties, the heteroclinic cycle persists. However, as one varies a system parameter ρ, β, λ_1 , and $\Delta_i, i = 1 \dots 14$, are likely to vary.

The crucial parameter here is ρ . If we have $\rho > 1$, the origin $a_1 = a_4 = a_5 = 0$ of the map is stable, which implies a stable heteroclinic cycle. However, if $\rho < 1$ then there exist infinitely many unstable periodic orbits (see Fig. 8) and a chaotic invariant set corresponding to shift dynamics on an infinite set of symbols (L, R -left or right spatial shift). Note that the Shil'nikov nature of the map only exists if $\beta \neq 0$. For $\beta = 0$, the map reduces to the standard map for heteroclinic cycles in the $O(2)$ -equivariant normal form. Note here though, that the condition on temporal stability is weaker than the one given by Armbruster *et al.* [2].

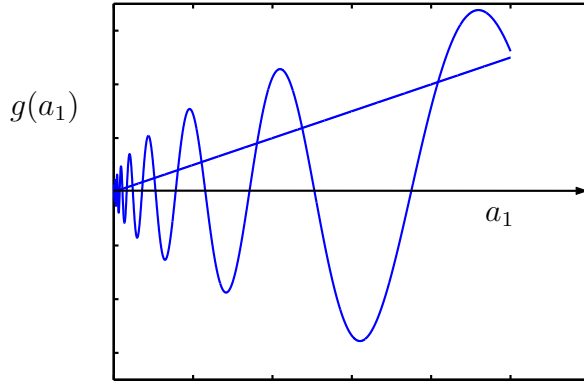


Fig. 8. Plot of the left side of the a_1 component of (22) versus $|a_1|$ for $\rho < 1$ showing many periodic solutions which are given by fixed points of the approximate 1D map.

3.3 Comparison with numerics

We are now in a position to answer the mystery of why the period of the heteroclinic cycles is small. Numerically, we approach the invariant subspaces Z_2 and \tilde{Z}_2 to within numerical error ($\sim 10^{-8}$), but the time spent at the equilibria is $T \sim 1/\lambda_1 \ln(1/\epsilon)$, where ϵ is the numerical tolerance. For our typical heteroclinic cycle $\lambda_1 = 82 \gg 1$ and so the time spent at the equilibria is very small (~ 0.5) regardless of the numerical tolerance. In order to demonstrate the effect of the numerical error on the time spent at the equilibria we shall look at numerical simulations of the heteroclinic cycles for $R = 150, \nu = 0.5, \mu = -4$ for two different numerical tolerances. For these equation parameters $\lambda_1 \approx 22.11$. In Fig. 9(a), we see two plots of the heteroclinic cycle for $\text{TOL} = 10^{-5}$ (shown as a dashed line) and $\text{TOL} = 10^{-14}$ (solid line). For the lower tolerance simulation we see that the time spent at

the equilibria is $T \approx 0.5$ whereas $T \approx 1.1$ for the higher tolerance simulation. These times are consistent with our Poincaré return map approximation for the time spent at the equilibria where $T \sim 1/\lambda_1 \ln(1/10^{-5}) = 0.5207$ for the lower tolerance, and $T \sim 1/\lambda_1 \ln(1/10^{-14}) = 1.4580$, for the higher tolerance ($T \sim 1/\lambda_1 \ln(1/10^{-10}) = 1.0414$). In Fig. 9(b), we have plotted the quantity $\ln(\text{Re}\{W_{-1} - W_1\})$ to show how the simulations approach the Z_2 -subspace to within numerical error i.e., $\ln(\text{Re}\{W_{-1} - W_1\}) \approx -30$ numerical error 10^{-14} . In Fig. 9, we see the characteristic ‘slowing-down’ of the heteroclinic cycle for odd initial conditions. Here $\rho = 8.36$ so we observe rapid convergence to the heteroclinic cycle, but for smaller ρ we find a longer period of slowing down.

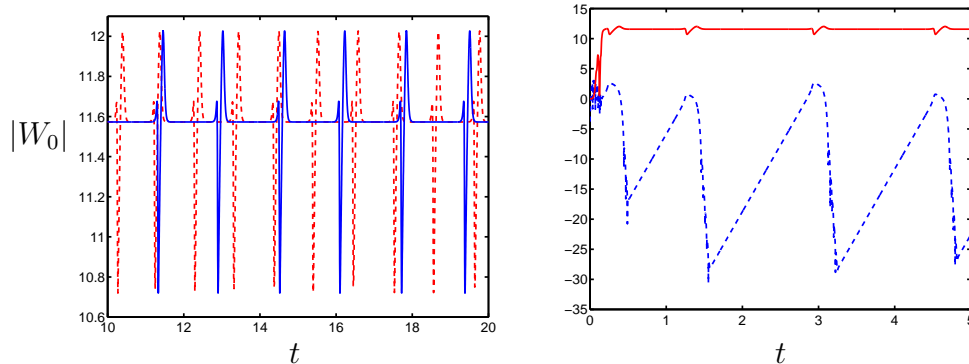


Fig. 9. Panel (a) shows a numerical simulation of the heteroclinic cycles for $R = 150, \nu = 0.5, \mu = -4$ with two different tolerances. The dashed line shows the simulation of the heteroclinic cycle with a tolerance of 10^{-5} at the equilibria and the solid line with a tolerance of 10^{-14} at the equilibria. Note that the period between burtings is smaller for the dashed line. Time spent at the equilibria for $\text{TOL} = 10^{-14}$ time spent at equilibria $T \sim 0.5$ and for $\text{TOL} = 10^{-10}$ $T \sim 1.1$. Panel (b) shows a plot of $|W_0|$ shown as a solid line and $\ln(\text{Re}\{W_{-1} - W_1\})$ (dashed line) for the heteroclinic cycle starting from odd initial conditions. Note the initial lengthening of the period.

In Fig. 10, we plot the value of ρ for $\nu = 1, \mu = -4$ for $R = 50..140$, passing though the parameter region where our ‘typical’ heteroclinic cycle exists. Observe that we should see stable heteroclinic cycles for $R \in (68.68, 79.82)$ and $R \in (103.78, 117.77)$. At $R = 110.08$ we see another bifurcation where we have a 2 distinct, unstable (real) eigenvalues, associated with the unstable branch of equilibria, ξ_1 in the Z_2 -subspace. As R is increased further these two unstable eigenvalues collide and become complex conjugate, resulting in a bifocal-heteroclinic cycle, before we eventually see a Hopf bifurcation at $R = 117.77$ in the 5-mode truncation. One would still expect though that the quantity $\rho = \alpha/\text{Re}(\lambda_1)$ still governs stability of the cycles. In the next section we shall discuss the bifocal heteroclinic cycle and the Hopf bifurcation.

Using the condition $\rho > 1$ for asymptotic stability, we can use numerical

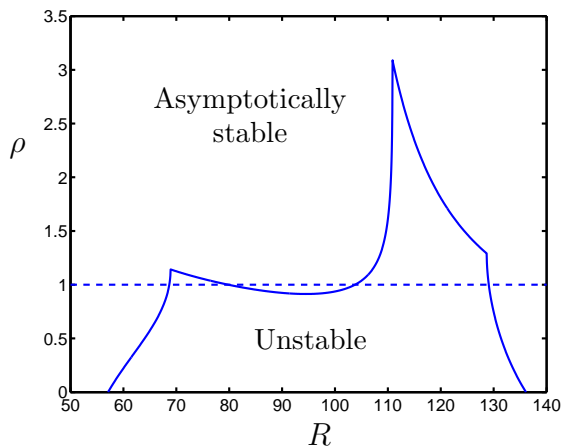


Fig. 10. Computation of the ratio $\rho = -\alpha/\lambda_1$ for $N = 2$ and $\nu = 1, \mu = -4$ and $R = 60 \dots 120$ demonstrating stability of the heteroclinic cycle.

continuation to trace out in two parameters, the stability region for the heteroclinic cycles defined by $\rho = 1$. To do this we continue one branch of the equilibria in the Z_2 -subspace and calculate the eigenvalues associated with the odd modes. This calculation is made easier by the fact that the eigenvectors associated with the radial-eigenvalues (i.e W_0 and W_2) are orthogonal to the eigenvectors associated with the odd Fourier modes (i.e W_1) and so the Jacobian can be decomposed into two block matrices, one associated with the radial-eigenvalues and the other with the odd Fourier modes; see Section 4. In order to calculate either α or λ_1 , we need to only find the maximum eigenvalue of the matrix associated with the odd Fourier modes evaluated along one branch of the equilibria (ξ_1 or ξ_2). The other eigenvalue, allowing us to calculate ρ , can be found by using $T_{1/4}$ to find the other equilibrium and evaluating the same block matrix associated with the odd Fourier modes, as we continue along one branch of equilibria.

Continuing in R and ν while $\rho = 1$, yields a two parameter bifurcation diagram for $\mu = -4$, shown in Fig. 11. Fig.12 shows a particular solution inside each of the open parameter regions of Fig.11. From Fig. 11, we can see that as $\nu \rightarrow 0.25$, the loci for existence and stability of the heteroclinic cycle tends to the $R_{crit}^{4\pi}$ locus. This suggests that a centre-unstable manifold reduction would be useful in analysing the heteroclinic cycles in this region of parameter space. As we have mentioned before, this calculation is highly involved even with the use of computer algebra software, suggesting that we need to go back and look at a reduction of the full PDE first before entering Fourier space. In Fig. 13, we see the evolution of a heteroclinic cycle close to the spatially homogeneous rotating wave in the region where a centre-unstable manifold reduction we be useful. Note here that the dynamics is constrained in a small region around the rotating wave solution, for which $|W_0| = \sqrt{R}$.

Let us now consider in more detail what is observed numerically in region (c)

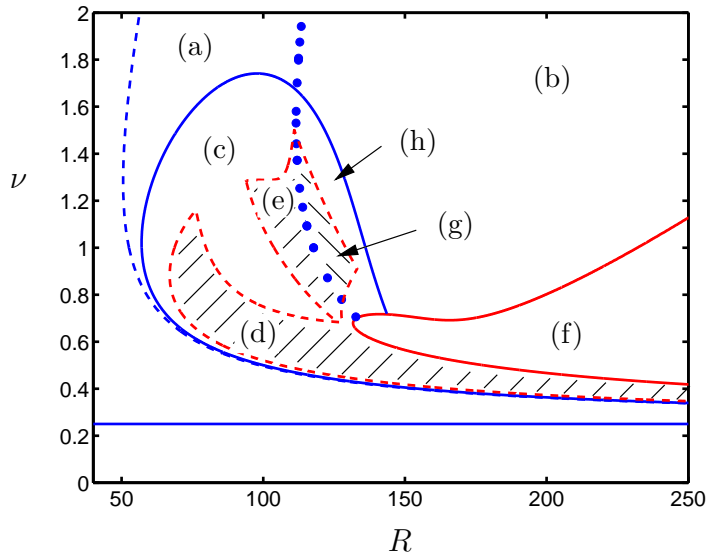


Fig. 11. Bifurcation diagram for $\mu = -4$ (see Fig 6). Asymptotically stable heteroclinic cycles can be found in shaded regions (d) and (e). Plots of the spatial average mode W_0 against time for (a), (b), (c), (d), (e), (f), (g), and (h) are shown in the corresponding panels of Fig. 12.

of Fig.11 where heteroclinic cycles exist but $\rho < 1$. Fig. 14 shows heteroclinic cycles for $R = 70$ and $R = 90$, $\nu = 1$, $\mu = -4$ in the (a_0, a_1) -plane, where $a_0 = W_0$ and $a_1 = \text{Re}(W_1)$. The linearisation about the heteroclinic points for both $R = 70$ and $R = 90$ is of the form described in Section 3.2. For $R = 70, \nu = 1, \mu = -4$, we have $\rho = \alpha/\lambda_1 \approx 1.12$ implying asymptotic stability and a unique heteroclinic cycle. In Fig 14(a), we see only one heteroclinic cycle for $R = 70$, but for $R = 90$, where $\rho = \alpha/\lambda_1 \approx 0.92$, we see in Fig 14(b) what appears to be chaotic dynamics close to the now unstable heteroclinic cycle, as predicted by the analysis of the 1D map (22) for $\rho < 1$.

The situation is not as simple as this since we also have the possibility of competing (chaotic)-attractors in the CGL. In Fig. 15 we see a case where $\rho = 1.05$, the heteroclinic cycle appears to attract dynamics from the zero solution before eventually the trajectory becomes chaotic.

3.4 Other heteroclinic dynamics

Let us now turn to an explanation of the observed dynamics in region (e) of Fig. 11, before the Hopf bifurcation. In this region we find that the heteroclinic cycles have a 2D unstable manifold. The construction of the Poincaré return map follows in much the same manner as before. The main difference here is that we now have a 2D unstable manifold that is the simple eigendirection associated with the real eigenvalue λ_1 replaced with a 2D space associated with complex eigenvalues $\lambda_1, \bar{\lambda}_1$ where $\text{Re}(\lambda_1) > 0$. Hence, the linearisation

about the heteroclinic points must change as well as the connecting global diffeomorphism ϕ . For the sake of brevity we do not carry out the analysis here, but from the results of Krupa and Melbourne [19], we see that the saddle quantity $\rho = \alpha/\text{Re}(\lambda_1)$, governs the stability of the heteroclinic cycle. Ashwin and Chossat [7] have studied homoclinic cycles with a 2D unstable manifold. They show that, if the cycle is asymptotically stable and all the expanding eigenvalues are real, then there exists a subcycle tangent to the strong unstable direction which attracts most of the trajectories, but does not satisfy the conditions for asymptotic stability. When the unstable eigenvalues become complex, as in the CGL, Ashwin and Chossat [7] provide evidence that the basin of attraction of the subcycle is riddled. We leave exploration of this possibility of a subcycle for future work.

Let us now turn to an explanation of the observed dynamics in region (g) and (h) of Fig. 11 beyond the Hopf bifurcation. At $R = 117.11, \nu = 1, \mu = -4$, the equilibria (ξ_1, ξ_2) involved in the stable heteroclinic cycles, undergo a Hopf bifurcation. The simulation in Fig. 16, suggests that after this Hopf bifurcation a limit-cycle to limit-cycle heteroclinic cycle can be observed. In the full PDE, these solutions correspond to connections on a two-frequency invariant torus related by a $1/4$ spatial symmetry in the amplitude. Since the Hopf-bifurcation is due to (invariant) radial-eigenvalues crossing the imaginary-axis, the structural stability and robustness of the cycles is still preserved since the two invariant subspaces (Z_2 and \tilde{Z}_2) still intersect at the limit-cycles (i.e. $W_{-1} = W_1 = 0$ at the limit-cycles). Since the Hopf bifurcation occurs in the direction associated with the radial eigenvalues the heteroclinic cycle can remain stable upto the bifurcation, unlike the standard Shil'nikov-Hopf bifurcation for non-equivariant systems.

We can construct a return map valid in a neighbourhood of the boundary between region (e) and (g) e.g., similarly to the approach used by Hirschberg and Knobloch [15] for the standard Shil'nikov-Hopf bifurcation. For brevity we omit the details, although it is clear that the saddle quantity ρ still to govern the stability of the heteroclinic cycles, close to the Hopf bifurcation. The shaded region (g) in fig 11 is defined by $\rho = 1$, in terms of the eigenvalues of the equilibria rather than the Floquet multipliers of the limit cycles. We have still found though that the boundary is fairly sharp and that in region (h) we find no stable heteroclinic cycles.

As well as observing stable limit-cycle to limit-cycle, heteroclinic cycles in region (g) of Fig. 11 corresponding to $\rho > 1$, we also find a region (h), where $\rho < 1$ immediately before the Hopf bifurcation. Here one can find a variety of different dynamics in particular heteroclinic cycles interrupted by regions of chaos; see Fig. 17. The dynamics here are reminiscent of a blow-out bifurcation since we have an invariant sub-manifold on which heteroclinic dynamics evolve; see Ashwin *et al.* [5]. This invariant sub-manifold has a locally riddled

basin of attraction. We can see this from Fig. 17 (c), where we have plotted the invariant quantity for the heteroclinic cycles (without decoupled phase), $|W_{-2}| - |W_2|$. This quantity should be zero if we are evolving in the invariant sub-manifold containing the heteroclinic cycles. We see that this quantity intermittently becomes chaotic, signifying a transverse instability and then becomes zero again with the dynamics relaxing back to the heteroclinic cycle.

4 Heteroclinic cycles in the full PDE

We can use the results from the Fourier 5-mode truncation to help guide an explanation of the heteroclinic cycles that are observed in the full CGL. The invariant \mathbb{Z}_2 -subspaces that the heteroclinic cycles evolve in are defined by the subspace of solutions even about $x = 1/2$ (Z_2) and $x = 1/4$ (\tilde{Z}_2). Hence, in Fourier space $Z_2 = \{W_{-n} = W_n, n \neq 0\}$ and $\tilde{Z}_2 = \{W_{-n} = W_n, n \text{ even}, W_{-n} = -W_n, n \text{ odd}\}$ (i.e., $T_{1/2}Z_2 = \tilde{Z}_2$), where W_n are the Fourier modes. In Fourier space, all the odd modes are zero at the equilibria. This can be seen by looking at the equilibria that are equivariant under $T_{1/2}$. Applying $T_{1/2}$ to the Fourier expansion yields

$$\begin{aligned} T_{1/2}u(x) &= \sum_{n=-\infty}^{n=+\infty} W_n(t)\exp(i2\pi n(x + 1/2)), \\ &= \sum_{n=-\infty}^{n=+\infty} (-1)^n W_n(t)\exp(i2\pi nx). \end{aligned} \quad (23)$$

We see that the right-hand side of (23) can only equal the left-hand side if and only if $W_n = 0$ for n odd.

The following two lemmas show that the structure of the subspaces in the 5-mode truncation is preserved in the infinite-dimensional projection. The first lemma generalises the result that equations (13) are equivariant under $T_{1/4}$. The second lemma shows that the Jacobian of the heteroclinic equilibria can be decomposed into two block matrices, one associated with the even modes and the other with the odd modes. These two lemmas then allow us to define stability criteria for the heteroclinic cycles in arbitrary-order truncations.

Lemma 1 *In the fixed point subspace of $T_{1/2}$, the spatial translation of $x = 1/2$, equation (7)*

$$\dot{W}_n = (R - (2\pi n)^2(1 + i\nu))W_n - (1 + i\mu) \sum_{k-l+m=n} W_k \bar{W}_l W_m,$$

is equivariant under $T_{1/4}$.

Proof: We can simply just consider the restriction of $T_{1/2} \circ R_f$ where all odd Fourier modes are zero. Hence, we need only consider $n \geq 0$, see (23). Consider the equation,

$$\dot{W}_{2n} = (R - (2\pi n)^2(1 + i\nu))W_{2n} - (1 + i\mu) \sum_{k-l+m=2n} W_k \bar{W}_l W_m. \quad (24)$$

Now $T_{1/4}W_{2n} \mapsto [W_0, -W_2, \dots, W_{4n}, -W_{2(2n+1)}, \dots]$. It is trivial to show that the linear part of (24) is equivariant under $T_{1/4}$. If $T_{1/4}W_{4n} \mapsto W_{4n}$ then we need to show,

$$T_{1/4} \sum_{k-l+m=4n} W_k \bar{W}_l W_m = \sum_{k-l+m=4n} W_k \bar{W}_l W_m.$$

Since k, l and m must be even and either $k = 2(2k + 1), l = 2(2l + 1), m = 2(2m + 1)$ or $k = 4k, l = 4l, m = 4m$, we only have three possible combinations of k, l , and m which leave the summation (25) invariant. This can be seen by examining

$$T_{1/4} \sum_{k-l+m=4n} W_k \bar{W}_l W_m = - \sum_{k-l+m=4n} W_k \bar{W}_l W_m,$$

then we must have $k = 2(2k+1), l = 4l, m = 4m$ etc., but $2(2k+1) - 4l + 4m = 4n \Rightarrow 2(2(k-l+m) + 1) = 2(2n)$, which is not possible. Similarly, we can show that

$$T_{1/4} \sum_{k-l+m=2(2n+1)} W_k \bar{W}_l W_m = - \sum_{k-l+m=2(2n+1)} W_k \bar{W}_l W_m.$$

□

In Lemma 2, we show that the eigenvectors of the odd Fourier modes are orthogonal to the eigenvectors of the even and spatial average modes, by looking at the Jacobian row for W_n of the Fourier projection without decoupled phase (7).

Lemma 2 *Let \mathbf{x} be the vector of all even Fourier modes and their complex conjugate (including W_0 -mode) and \mathbf{y} be the vector of all odd Fourier modes and their complex conjugate, such that,*

$$\mathbf{x} = [\dots, W_{-2n}, \bar{W}_{-2n}, \dots, W_0, \bar{W}_0, \dots, W_{2n}, \bar{W}_{2n}, \dots] \text{ and}$$

$$\mathbf{y} = [\dots, W_{-2n+1}, \bar{W}_{-2n+1}, \dots, W_{-1}, \bar{W}_{-1}, W_1, \bar{W}_1, \dots, W_{2n+1}, \bar{W}_{2n+1}, \dots].$$

Define $\mathbf{X} = [\mathbf{x}, \mathbf{y}]$, then the linearisation of (7) about equilibria, ξ_1 and ξ_2 , invariant under $T_{1/2}$, has the form

$$\dot{\mathbf{X}} = \begin{pmatrix} J_e & 0 \\ 0 & J_o \end{pmatrix} \mathbf{X}, \quad (25)$$

where J_e is the Jacobian of the even, (\mathbf{x}), Fourier modes and J_o is the Jacobian of the odd, (\mathbf{y}), Fourier modes. Furthermore, the linearisation $\dot{\mathbf{x}} = J_e \mathbf{x}$ is $T_{1/4}$ -equivariant but $\dot{\mathbf{y}} = J_o \mathbf{y}$ is not.

Proof: We need only consider the n 'th equation of (7) since \overline{W}_n can be found by complex conjugation of (7). The n 'th row of the Jacobian of (7) is defined by $J_{n,2j} = \partial \dot{W}_n / \partial W_j$ and $J_{n,2j+1} = \partial \dot{W}_n / \partial \overline{W}_j$, where

$$\frac{\partial \dot{W}_n}{\partial W_j} = (R - (2\pi n)^2(1 + i\nu)) - 2(1 + i\mu) \sum_{m-l=n-j} \overline{W}_l W_m \quad j = n, \quad (26)$$

$$= -2(1 + i\mu) \sum_{m-l=n-j} \overline{W}_l W_m \quad j \neq n, \quad (27)$$

$$\frac{\partial \dot{W}_n}{\partial \overline{W}_j} = -(1 + i\mu) \sum_{k+m=n+j} W_k W_m. \quad (28)$$

Using the fact that all odd modes are zero for equilibria invariant under $T_{1/2}$, we see that for all three summations above to be non-zero they must only include even modes, i.e., k, l, m must be even integers. Let us look first at the summation (27). If m and l are even integers then so are $m - l$ and hence $n - j$. So the parity of j is the same as the parity of n . This is also true for (26) and (28). Hence for all even W_n -modes, all the odd terms in the Jacobian are zero and visa versa for the odd W_n -modes. So the linearisation about even equilibria that are invariant under $T_{1/2}$ has the form (25).

Using Lemma 1, we see that the linearisation $\dot{\mathbf{x}} = J_e \mathbf{x}$ is invariant under $T_{1/4}$.

Taking (27), we see that $m - l = 2n + 1 - (2j + 1) = 2(n - j)$ or $m - l = 2n + 1 + (2j + 1) = 2(n + j) + 2$. Hence, the summation has even and odd terms so that $J_o T_{1/4} \mathbf{y} \neq T_{1/4} J_o \mathbf{y}$. \square

Hence, the \mathbb{Z}_2 subspaces and the heteroclinic equilibria seen in the 5-mode truncation maintain their structure in the full PDE allowing for structurally stable heteroclinic cycles to exist in the infinite-dimensional ODE system.

We can now state the main result of this section that will allow us to trace out a bifurcation diagram in higher Fourier truncations.

Theorem 1 *For R sufficiently close to $R_{crit}^{4\pi}$ there exists 2 solutions (ξ_1 and ξ_2) to*

$$\dot{W}_n = (R - (2\pi n)^2(1 + i\nu))W_n - (1 + i\mu) \sum_{k-l+m=n} W_k \overline{W}_l W_m, \quad (29)$$

that are $T_{1/2}$ -equivariant and are related by $T_{1/4}\xi_1 \mapsto \xi_2$. The linearisation

about either ξ_1 or ξ_2 is of the form

$$\dot{\mathbf{X}} = \begin{pmatrix} J_e & 0 \\ 0 & J_o \end{pmatrix} \mathbf{X}. \quad (30)$$

Furthermore, if there exists a robust connection in $\text{Fix}(\mathbb{Z}_2)$, such that $\xi_1 \rightarrow \xi_2$ then there exists a heteroclinic cycle that is asymptotically stable if

$$\rho = \frac{\max\{\text{Re}(\text{eig}[J_o|_{\xi_2}])\}}{\max\{\text{Re}(\text{eig}[J_o|_{\xi_1}])\}} > 1. \quad (31)$$

Proof: Following the work of Takac [38], at $R_{crit}^{4\pi}$ we see that the centre-eigenspace is spanned by $\{e^{-i4\pi x}, e^{i4\pi x}\}$. Hence, we have the parameterised family of centre-manifolds as graphs of the form

$$W_n = h_n(W_{-2}, W_2, R, \nu, \mu), \quad n \neq -2 \text{ or } 2. \quad (32)$$

Therefore, the centre-manifold is $T_{1/2}$ -equivariant ($T_{1/2}h_n(W_{-2}, W_2, R, \nu, \mu) = h_n(W_{-2}, W_2, R, \nu, \mu)$), hence all the odd Fourier modes are zero. Since we have a pitchfork bifurcation (see Takac [38]), we have two new solutions ξ_1 and ξ_2 related by $T_{1/4}$ (or $T_{3/4}$). Using Lemma 2, we see that the linearisation about either ξ_1 or ξ_2 has the form (25).

A robust connection from $\xi_1 \rightarrow \xi_2$ in $\text{Fix}(\mathbb{Z}_2)$ implies that in, say, $\text{Fix}(\mathbb{Z}_2)$ ξ_1 is linearly unstable and ξ_2 is linearly stable and there is a connection $\xi_1 \rightarrow \xi_2$. From Section 3.1 we see that such a connection implies a heteroclinic cycle ($\xi_1 \mapsto \xi_2 \mapsto \xi_1$). The condition for asymptotic stability of the cycle is found using the results of Krupa and Melbourne [18]. \square

Our results on the temporal stability of the heteroclinic cycles carry through unchanged since the Poincaré map analysis in Section 3.2 is defined in terms of the set-up of the leading eigenvalues, ignoring directions corresponding to the strong stable and strong unstable, manifold. Hence, for $\rho < 1$ we would still expect to find infinitely-many heteroclinic cycles.

Theorem 1 allows us to use numerical continuation to trace out bifurcation loci corresponding to $\rho = 1$ for an arbitrary Fourier truncation. In Fig. 18, we plot a bifurcation diagram corresponding to a 13-mode truncation ($N = 6$). Here, for the values $\nu = 1, \mu = -4$, $R_{crit}^{4\pi}$ is identical to the 5-mode truncation, $R_{\text{Hopf}} = 120.02$ (showing an $O(1)$ difference from the five-mode truncation but within 10^{-2} of the true value found for high mode truncations). A fold locus passes through this region intersecting the Hopf locus at $R = 141, \nu = 0.7, \mu = -4$. At this point the Hopf bifurcation of the heteroclinic points no longer takes place and below this region we see a large region of parameter space where robust heteroclinic cycles exist. Note here that for $\nu = 1, \mu = -4$, the saddle quantity ρ

does not dip below 1, after the initial crossing, until after the Hopf bifurcation. This would suggest that the heteroclinic cycles in the full PDE should be asymptotically stable for the entire region, $R = 65 \dots 120, \mu = -4, \nu = 1$, unlike for the 5-mode truncation (c.f. Fig. 11). In the five-mode truncation for $R = 90, \nu = 1, \mu = -4$, Fig. 14 indicated that for $\rho < 1$, many heteroclinic cycles are observed. In Fig. 19, the 13-mode truncation we no longer see many heteroclinic cycles in the region where ρ dips below 1 in the 5-mode truncation.

5 Conclusion

In this paper we have described and explained the existence of robust heteroclinic cycles in the one-dimensional, complex Ginzburg-Landau equation posed on a spatially periodic domain. These cycles have provided us with many numerical and analytical problems which we have only begun to solve in this paper. Our approach has been to tackle these heteroclinic cycles in an intuitive manner based on observations made in the full PDE rather than looking *a priori* at heavy restrictions/truncations and seeing where they apply to the CGL. A combination of numerical and analytical techniques is then required to gain insight into the dynamics associated with these heteroclinic cycles.

The CGL is a well studied amplitude equation whose dynamics one might believe have been exhaustively studied [12,17,27,22] yet, we have found large parameter regions of new behaviour consisting of large quiescent periods of time-periodic solutions interspersed by rapid bursts causing a $1/4$ period shift, away from the arbitrarily chosen line $\mu = -\nu$ studied by most authors. For example, we have found a variety of Shil'nikov-type heteroclinic cycles including saddle-focus and bi-focal cycles as well as heteroclinic cycles between limit cycles. We have observed other instabilities due to perturbations outside the invariant subspaces which the heteroclinic cycles evolve in. In particular, we have found something akin to a blow-out bifurcation for the limit-cycle to limit-cycle heteroclinic cycle. For example in Fig. 20, we show the heteroclinic connection between ξ_1, ξ_2 and a new relative equilibria, for a 7-mode Fourier truncation with $R \approx 73.73, \nu = 1, \mu = -4$. This new heteroclinic bifurcation serves to show how rich the dynamics of the CGL in this parameter region are.

It would be interesting to study the onset of the cycles with local analysis. Most of the heteroclinic cycles require a high-dimensional phase space, but close to the $R_{crit}^{4\pi}$ bifurcation the cycles appear to be described by the dynamics of the 1:2 mode-interaction, $O(2)$ -equivariant normal form [2]. A centre-unstable manifold reduction of the Fourier truncation is not straightforward.

Also the dynamics would be governed by real eigenvalues rather than being of Shil'nikov-type. Perhaps a more promising approach would be to perform an analysis close to $R_{crit}^{4\pi}$ where the cycles have small amplitude modulations. Several reductions are possible here (e.g. sideband perturbation etc.), but perhaps the most promising reduction comes from the analysis of hole solutions and weak turbulence in the CGL by Lega [20]. She shows how to reduce the CGL formally by assuming that the amplitude is 'slaved' to phase when it is very much smaller than the amplitude of the spatially homogeneous rotating wave. This reduction effectively yields a Kuramoto-Sivashinsky equation with some extra nonlinearities. This is a particularly compelling equation to study since that KS-equation is known to support robust heteroclinic cycles, see Armbruster *et al.* [3], which could provide a local explanation of the birth of such cycles in the CGL close to $R_{crit}^{4\pi}$.

Another open problem is how to use numerical continuation to explore the global bifurcations of the heteroclinic cycles that we cannot find. The two continuous symmetries of the CGL (complex phase and spatial translation) provide significant challenges to numerical continuation techniques since they result in a multi-parameter family of solutions. Ashwin *et al.* [4,6], have adapted the numerical continuation scheme for continuation of homoclinic orbits by Champneys *et al.* [9], for continuation of homoclinic cycles in the Kuramoto-Sivashinsky equation. Further work will concentrate on adaption of these methods for the CGL and those of Muñoz-Almaraz *et al.* [31] on factoring out symmetries, in the Hamiltonian context, for numerical continuation.

Although all the presented numerical experiments have been confined to the case $\mu = -4$, further experiments not presented suggest the behaviour to persist for a large range of μ -values where the heteroclinic cycles exist in 'bubbles' of parameter space. Another interesting piece of evidence that points to the robustness of what we have observed is that using numerics we have found structurally stable heteroclinic cycles in the quintic CGL,

$$u_t = (1 + i\nu)u_{xx} + Ru - (1 + i\mu)|u|^4u,$$

which appear to have an even larger stability region than those for the cubic CGL. Several other open problems remain. For example, whether the equivalent of these heteroclinic cycles exists in higher spatial dimensions, what happens to the dynamics near forced symmetry breaking and what happens when other symmetries are imposed e.g., the CGL with a conservation law [23]?

Let us turn finally to possible physical applications. Heteroclinic cycles have been used to describe spatio-temporal intermittency in a variety of applications; see Krupa [18] for a review. For example, experiments on Taylor-Couette flow by Mullin *et al.* [30] have shown a wide variety of Shil'nikov-like behaviour as well as spatio-temporal intermittency close to the critical Reynolds number for the onset of rolls, at which the CGL is valid. Thus, the robust Shil'nikov

heteroclinic cycles that exist in the CGL could provide an explanation for the structure of the chaotic dynamics in the Taylor-Couette flow. More generally, spatio-temporal intermittency is a feature of many weakly turbulent fluid flows and the discovery of these new heteroclinic cycles in this paper might prove insisive in describing experiments where gradual transition to turbulence occurs, following an initial onset of patterned state. Finally, we remark that a modification to the CGL with rapidly-oscillating nonlocal terms has been shown rigorously by Melbourne [16] to be derived as a normal form close to the critical Reynolds number bifurcating directly from the Navier Stokes equation. It would be interesting to see therefore whether the robust structures we have computed, qualitatively survive under the addition of these nonlocal terms and therefore can be confidently connected to what is observed in fluid experiments.

Acknowledgements

D.L. would like to thank Phil Holmes, Vivien Kirk, Paul Matthews, Alastair Rucklidge, Edgar Knobloch, Dieter Armbruster, Ian Melbourne, Rebecca Hoyle, Ann Skeldon and Thomas Wagenknecht, for their help and many useful suggestions and comments. This work was supported by an EPSRC Research Studentship.

References

- [1] A.MIELKE, *Bounds for the solutions of the complex ginzburg-landau equation in terms of the dispersion parameters*, Physica D, 117 (1998), pp. 106–116.
- [2] D. ARMBRUSTER, J. GUCKENHEIMER, AND P. HOLMES, *Heteroclinic cycles and Modulated Travelling waves in systems with $O(2)$ symmetry*, Physica D, 29D (1988), pp. 257–282.
- [3] ———, *Kuramoto-Sivashinsky dynamics on the centre-unstable manifold*, SIAM J. APPL. MATH, 49 (1989), pp. 676–691.
- [4] P. ASHWIN, K. BOHMER, AND Z. MEI, *Forced symmetry breaking of homoclinic cycles in a pde with $O(2)$ symmetry*, Journal of Computational and Applied Mathematics, 70 (1996), pp. 297–310.
- [5] P. ASHWIN, J. BUESCU, AND I. STEWART, *From attractor to chaotic saddle: a tale of transverse instability*, Nonlinearity, 9 (1996), pp. 703–737.
- [6] P. ASHWIN AND Z. MEI, *A numerical bifurcation function for homoclinic orbits*, SIAM J. Numer. Anal., 35 (1998), pp. 2055–2069.

- [7] P. ASHWIN AND P. CHOSSAT, *Attractors for Robust Heteroclinic Cycles with Continua of Connections*, J. Nonlinear Sci., 8 (1998), pp. 103–129.
- [8] S. A. CAMPBELL AND P. HOLMES, *Bifurcation from $O(2)$ symmetric heteroclinic cycles with three interacting modes*, Nonlinearity, 4 (1991), pp. 697–726.
- [9] A. CHAMPNEYS, Y. KUZNETSOV, AND B. SANDSTEBE, *A numerical toolbox for homoclinic bifurcation analysis*, International Journal of Bifurcation and Chaos, 6 (1996), pp. 867–887.
- [10] B. DENG, *The Sil'nikov problem, exponential expansion, strong λ -lemma, C^1 -linearisation, and homoclinic bifurcation.*, J. Diff. Equat., 79 (1989), pp. 189–231.
- [11] E. DOEDEL, R. PAFFENROTH, A. CHAMPNEYS, T. FAIRGRIEVE, Y. KUZNETSOV, B. STANDSTEBE, AND X. WANG, *Auto 2000: Continuation and bifurcation software for ordinary differential equations (with homcont)*, tech. rep., Caltech, 2001.
- [12] A. DOELMAN, *Finite-dimensional models of the Ginzburg-Landau equation*, Nonlinearity, 4 (1991), pp. 231–250.
- [13] C. DOERING, J. GIBBON, D. HOLM, AND B. NICOLAENKO, *Low-dimensional behaviour in the complex Ginzburg-Landau equation*, Nonlinearity, 1 (1988), pp. 279–310.
- [14] P. GLENDINNING AND C. SPARROW, *Local and Global behaviour near homoclinic orbits*, Journal of Statistical Physics, 35 (1984), pp. 645–696.
- [15] P. HIRSCHBERG AND E. KNOBLOCH, *Sil'nikov-Hopf Bifurcation*, Physica D, (1993).
- [16] I. MELBOURNE, *Derivation of the time-dependent Ginzburg-Landau equation on the line*, J. Nonlinear Sci., 8 (1998), pp. 1–15.
- [17] L. KEEFE, *Dynamics of perturbed wavetrain solutions of the Ginzburg-Landau equation*, Stud. Appl. Math., 73 (1985), pp. 91–153.
- [18] M. KRUPA, *Robust Heteroclinic Cycles*, Journal of Nonlinear Science, 7 (1997), pp. 129–176.
- [19] M. KRUPA AND I. MELBOURNE, *Asymptotic stability of heteroclinic cycles in systems with symmetry.*, Ergodic Theory Dyn. Syst., 15 (1995), pp. 121–147.
- [20] J. LEGA, *Topological defects associated with the breaking of time translation invariance*, PhD thesis, University of Nice, 1989.
- [21] X.-B. LIN, *Using Melnikov's method to solve Silnikov's problems*, Proceedings of the Royal Society of Edinburgh, 116A (1990), pp. 295–325.
- [22] B. LUCE, *Homoclinic explosions in the complex Ginzburg-Landau equation*, Physica D, 84 (1995), pp. 553–581.

- [23] P. MATTHEWS AND S. COX, *Pattern formation with a conservation law*, Nonlinearity, 13 (2000), pp. 1293–1320.
- [24] I. MELBOURNE, P. CHOSSAT, AND M. GOLUBITSKY, *Heteroclinic cycles involving periodic solutions in mode interactions with $O(2)$ symmetry*, Proc. Roy. Soc. Edinburgh, 113A (1989), pp. 301–335.
- [25] I. MERCADER, J. PRAT, AND E. KNOBLOCH, *Robust Heteroclinic cycles in two-dimensional Rayleigh-Bénard Convection without Boussinesq symmetry*, International Journal of Bifurcation and Chaos, 12 (2002), pp. 2501–2522.
- [26] A. MIELKE, *Handbook of Dynamical Systems*, vol. 2, Elsevier, 2002, ch. 15.
- [27] H. MOON, P. HUERRE, AND L. REDEKOPP, *Transitions to chaos in the Ginzburg-Landau equation*, Physica D, 7 (1983), pp. 135–150.
- [28] K. MORTON AND D. MAYERS, *Numerical Solution of Partial Differential Equations*, Cambridge University Press, 1994, ch. 2.
- [29] M.R.E.PROCTOR AND C.A.JONES, *The interaction of two spatially resonant patterns in thermal convection. part1. exact 1:2 resonance*, J. Fluid Mech., 188 (1988), pp. 301–335.
- [30] T. MULLIN, *In Nonlinear Dynamics and Chaos*, IoP Publishing, 2003, ch. 7. Is chaos relevant to fluid mechanics?, pp. 167–187.
- [31] F. MUNOZ-ALMARAZ, E. FREIRE, J. GALÁN, E. DOEDEL, AND A. VANDERBAUWHEDE, *Continuation of periodic orbits in conservative and Hamiltonian systems*, Physica D, 181 (2003), pp. 1–38.
- [32] A. NEWELL AND J. WHITEHEAD, *Finite Bandwidth, Finite Amplitude Convection*, Journal of Fluid Mechanics, 38 (1969), pp. 279–304.
- [33] P. NEWTON, *Instabilities in the Ginzburg-Landau Equation*, PhD thesis, Brown university, 1986.
- [34] R.E.WILSON, *Numerically derived scalings for the complex ginzburg-landau equation*, Physica D, 112 (1998), pp. 329–343.
- [35] J. RODRIGUEZ AND M. SCHELL, *Global bifurcations into chaos in systems with $SO(2)$ symmetry*, Physics Letters A, 146 (1990), pp. 25–31.
- [36] A. RUCKLIDGE AND P. MATTHEWS, *Analysis of the shearing instability in nonlinear convection and magnetoconvection*, Nonlinearity, 9 (1996), pp. 311–351.
- [37] J. STUART AND R. DIPRIMA, *The Eckhaus and Benjamin-Fier resonance mechanisms*, Proc. R. Soc. A, 362 (1978), pp. 27–41.
- [38] P. TAKAC, *Invariant 2-tori in the time-dependent Ginzburg-Landau equation*, Nonlinearity, 5 (1992), pp. 289–321.

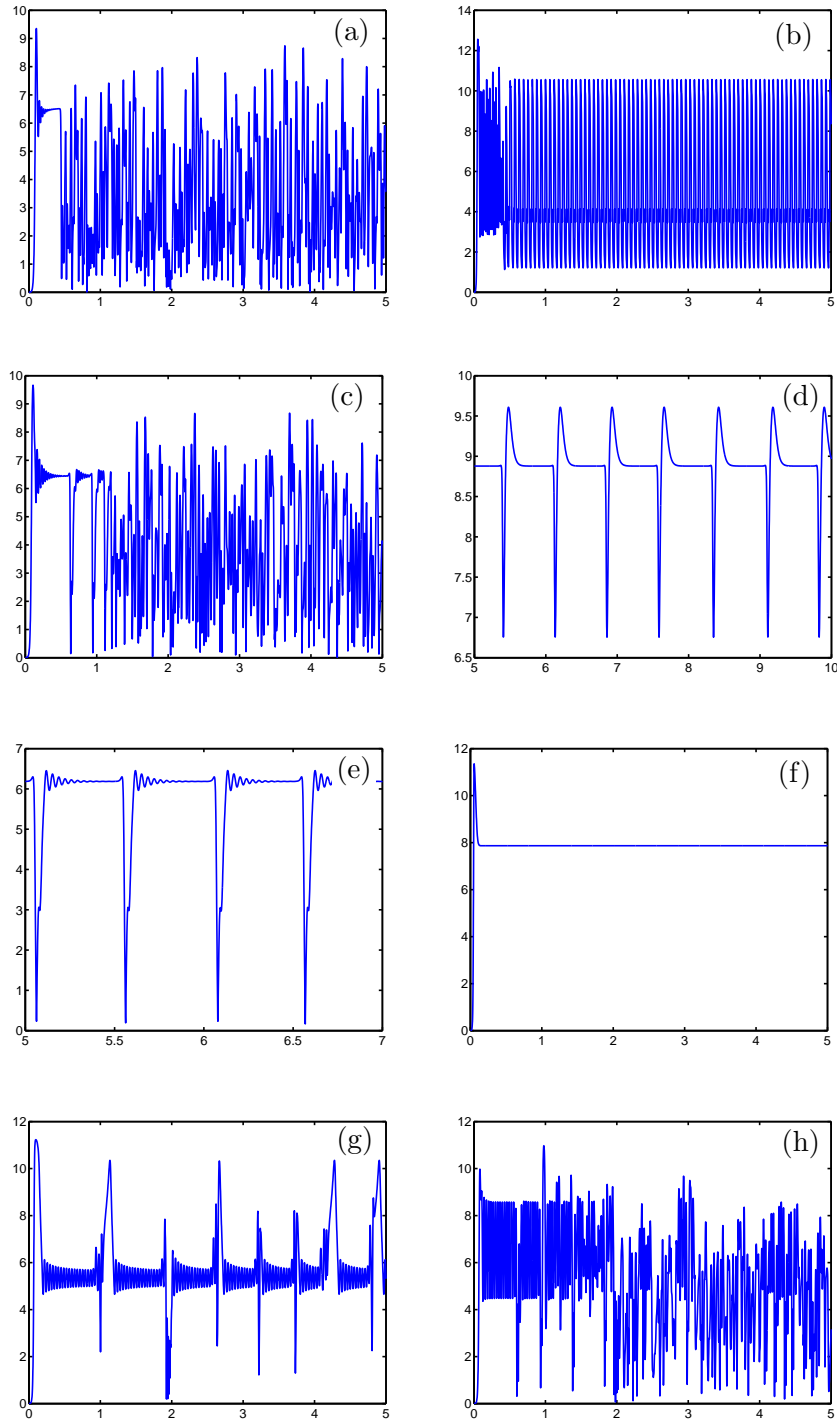


Fig. 12. Plots of the spatial average against time in the 5-mode Fourier truncation for the bifurcation diagram Fig.11 in regions (a)-(h). Panels (a), (c) and (h) show chaotic dynamics, (d), (e) and (g) show heteroclinic cycles. Panel (f) shows evolution to a the equilibria ξ_1 or ξ_2 .

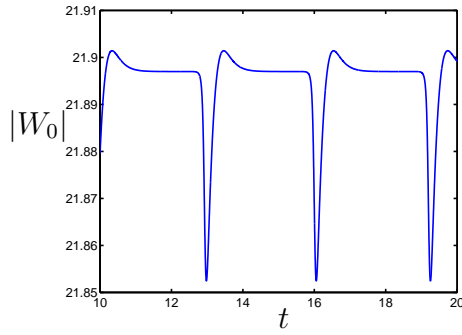


Fig. 13. Heteroclinic cycles for $R = 480, \nu = 0.3, \mu = -4$ close to $R_{crit}^{4\pi}$. Note the fluctuations of $|W_0|$ are very much smaller than the rotating wave $W_0 = \sqrt{R} \approx 21.9$.

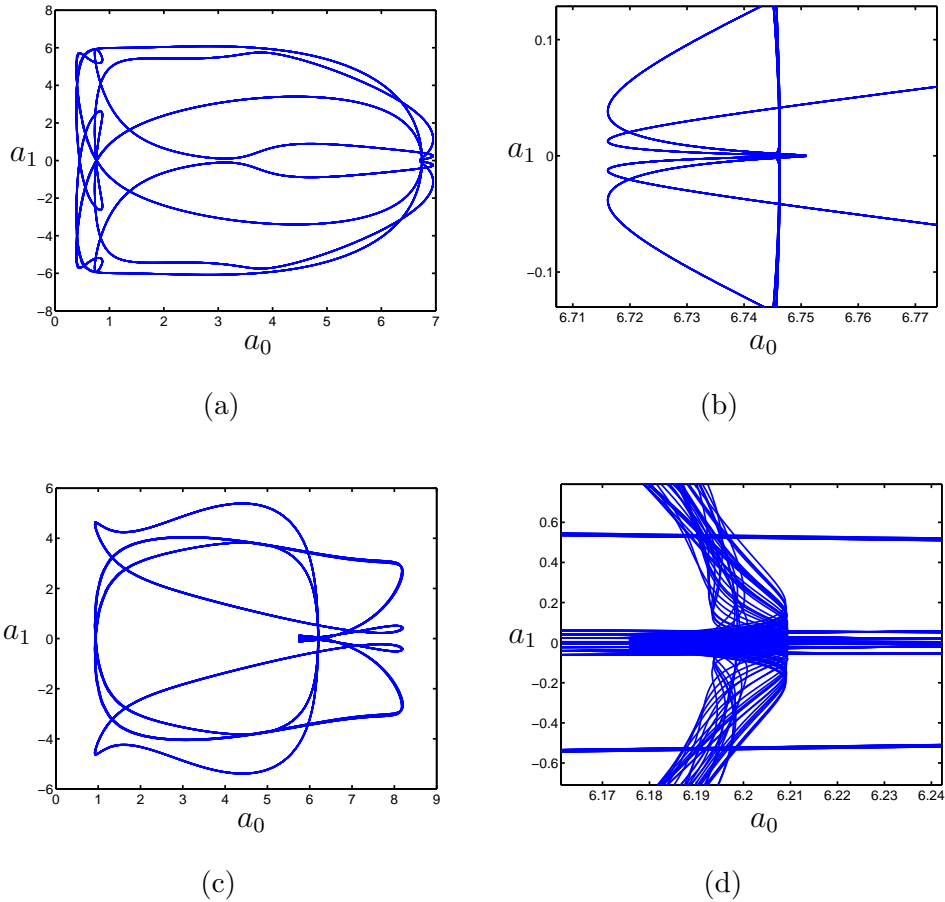


Fig. 14. Heteroclinic cycles in the (a_0, a_1) -Fourier plane for $\nu = 1, \mu = -4$ and (a),(b) $R = 70$ (for which $\rho = 1.12 > 1$) and (c),(d) $R = 90$ for which $\rho = 0.92$. Panels (b) and (d) show a zoom-in around the equilibria. In (b) we see only one heteroclinic cycle, but in (d) we see a large number of cycles.

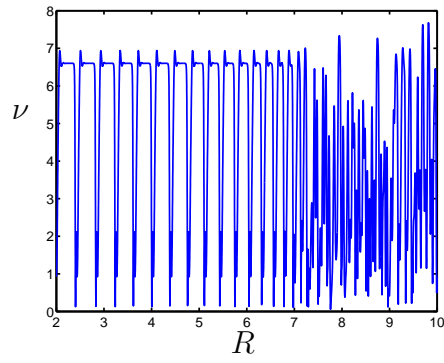


Fig. 15. Competing attractors for $R = 75, \nu = 1, \mu = -4, \rho \approx 1.05$.

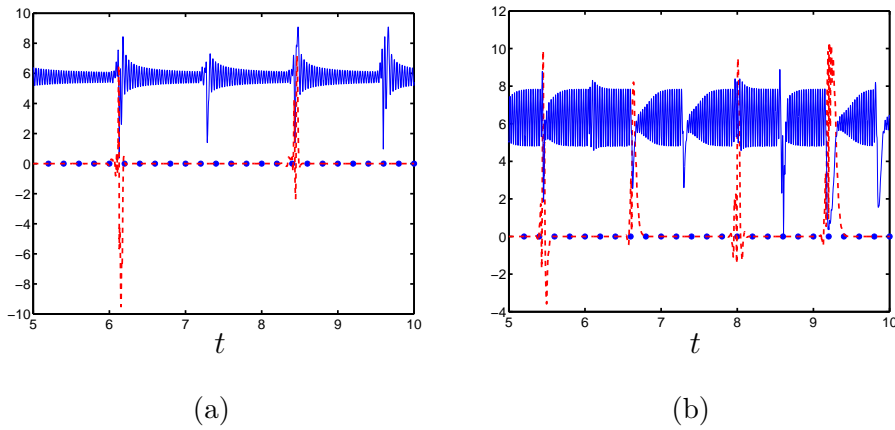


Fig. 16. Examples of a limit cycle to limit cycle heteroclinic connection, (a) $R = 118, \mu = -4, \nu = 1$ and (b) $R = 120, \mu = -4, \nu = 1.2$. W_0 is plotted as a solid line, $W_{-1} - W_1$ is shown as a dashed line and $W_{-2} - W_2$ is a dotted line.

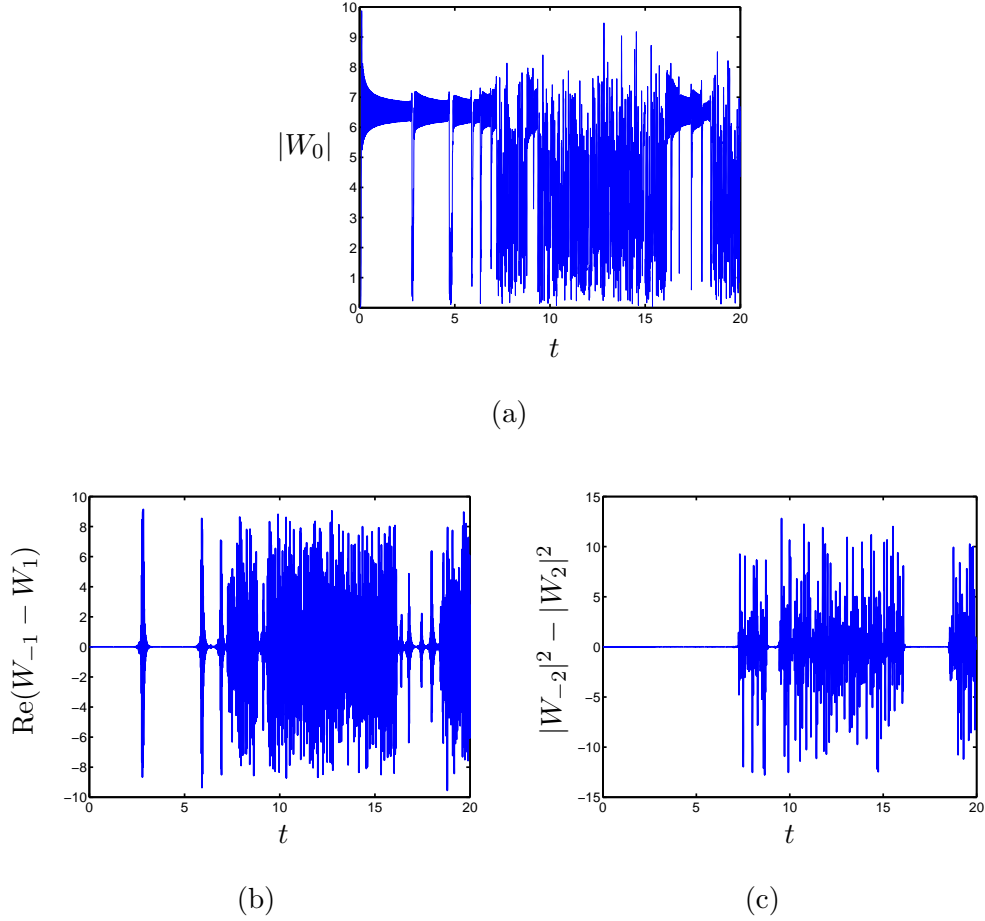


Fig. 17. Competing attractors, limit-cycle to limit-cycle heteroclinic cycle and spatio-temporal chaos. Phase is not decoupled. $R = 111.7$, $\nu = 1.5$, $\mu = -4$. The saddle quantity is $\rho = 0.88$. Panel (c) shows the invariant quantity for the heteroclinic cycles ($|W_{-2}|^2 - |W_2|^2$) becoming chaotic, implying a blow-out bifurcation.

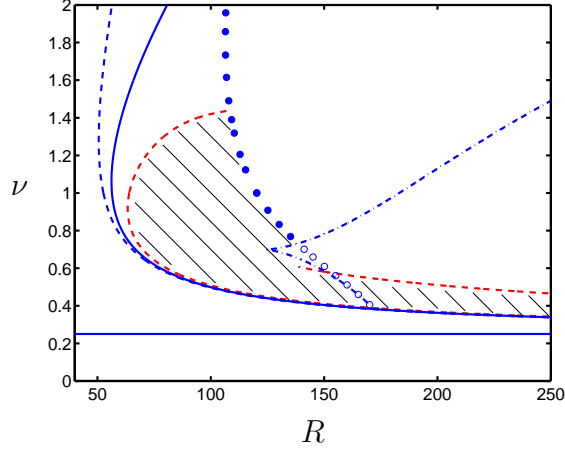


Fig. 18. Bifurcation diagram $N = 6$, $\mu = -4$. Asymptotically stable heteroclinic cycles can be found in the shaded region. Open blue circles denote Hopf-locus after a fold (shown as dashed/dotted line).

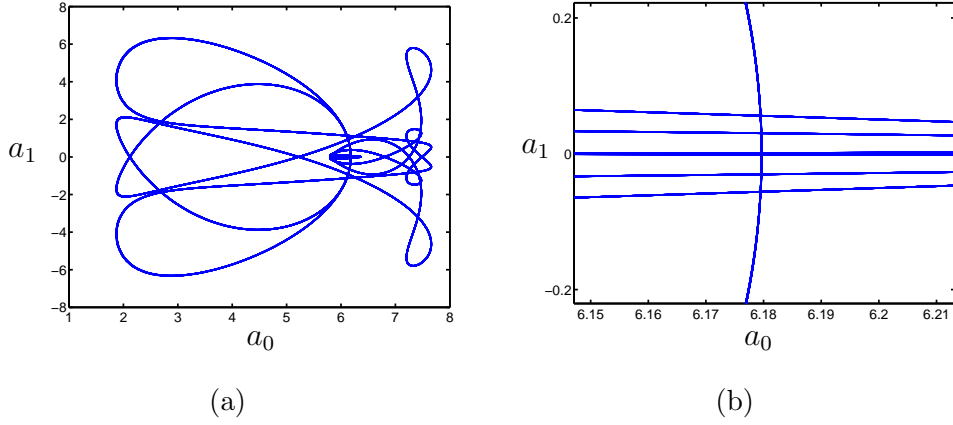
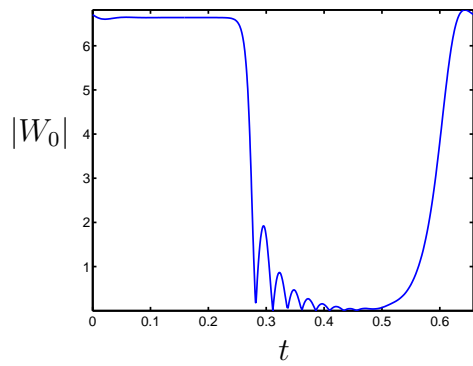
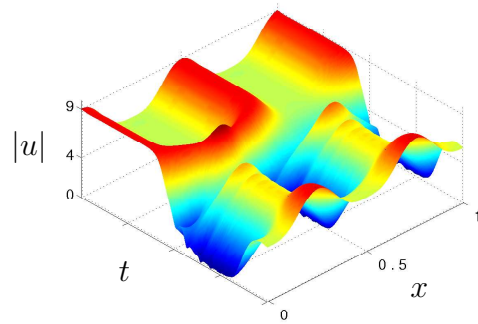


Fig. 19. Heteroclinic cycles in the (a_0, a_1) -Fourier plane for $R = 90, \nu = 1, \mu = -4$ in the 13-mode truncation. Panel (b) shows a zoom-in around the equilibria. In (b) we observe only one heteroclinic cycle compare with fig 14(d).



(a)



(b)

Fig. 20. A degenerate heteroclinic cycle for a 7-mode truncation (i.e. $N = 3$), $R = 73.7264$, $\nu = 1$, $\mu = -4$. Here the phase has not been decoupled since $|W_0| \rightarrow 0$. A connection to $W_0 = 0$ occurs in between the heteroclinic connections between ξ_1 and ξ_2 .